Physical Nature of Cytoplasm

Physical Nature of Cytoplasm

A dissertation presented

by

Ming Guo

to

The School of Engineering and Applied Sciences

in partial fulfillment of the requirements

for the degree of

Doctor of Philosophy

in the subject of

Applied Physics

Harvard University

Cambridge, Massachusetts

April 2014

Thesis Advisor
David A. Weitz

Author
Ming Guo

Physical Nature of Cytoplasm

Abstract

Forces are increasingly recognized as major regulators of cell physiology and function, and the mechanical properties of cells are essential to the mechanisms by which cells sense forces, transmit them to the cell interior or to other cells, and transduce them into chemical signals that impact a spectrum of cellular responses. Furthermore, cells can sense their extracellular environment and regulate their own mechanics and biology. Due to limitation of methodology, the cortical property of cells has been extensively characterized; however, the mechanics and dynamics of cytoplasm which consists all key cellular organelles, remains poorly understood. Moreover, a basic understanding of cell mechanics, such as which parameters correlates with cell stiffness and therefore impact cell biology is unknown. In this thesis, we firstly present a thorough investigation of the mechanical and dynamic properties of the cytoplasm, including direct measurement of cytoplasmic material property using optical tweezers, and visualization of intracellular dynamics by tracer particles. By combining these two measurements we obtain a directly characterization of the cytoplasmic forces; we further apply this method to study cancer cells and cells without vimentin intermediate filament, and find that cancer cells have significantly stronger intracellular forces, which vimentin intermediate filament does not have effect on the force generation. Secondly, we present our result on the role of cell

volume in cell mechanics and cell biology. We show that the volume of a cell changes upon the property of the extracellular environment; the change in cell volume directly induces change in the mechanical property of both cytoplasm and cell cortex. We further show that the change in cell volume is due to intracellular water influx/efflux, and this has significant impact on cell biology, such as stem cell differentiation. Finally, we present a direct characterization of the equation of state of living cells by measuring cell volume under increasing osmotic pressure. We show that a living cell, under osmotic compression, behaves as Van der Waals gas with a hard sphere excluded volume; the minimum volume of cells is determined by cellular proteins, which the equation of state of living cells is dominated by intracellular ions.

Contents

List of Figures

Citations to Previously Published Work

Large portions of Chapters 3 have appeared in the following paper:

"The Role of Vimentin Intermediate Filaments in Cortical and Cytoplasmic Mechanics", Ming Guo, Allen J. Ehrlicher, Saleemulla Mahammad, Hilary Fabich, Mikkel H. Jensen, Jeffrey R. Moore, Jeffrey J. Fredberg, Robert D. Goldman, David A. Weitz, Biophsical Journal, 105, 1562-1568 (2013).

Large portions of Chapters 4 have appeared in the following 3 papers:

"Probing the stochastic, motor-driven properties of the cytoplasm using force spectrum microscopy", Ming Guo, Allen J. Ehrlicher, Mikkel H. Jensen, Malte Renz, Jeffrey R. Moore, Robert D. Goldman, Jennifer Lippincott-Schwartz, Frederick C. Mackintosh, David A. Weitz, submitted to Cell.

"Identifying directional persistence in intracellular particle motion using Hidden Markov Models", Magnus Röding, Ming Guo, David A. Weitz, Mats Rudemo, Aila Särkkä, Mathematical Biosciences, (2014)

“Activity Driven Fluctuations in Living Cells”, E. Fodor, M. Guo, N.S. Gov, P. Visco, D. A. Weitz, and F. van Wijland， submitted to PRL

Large portions of Chapters 5 have appeared in the following paper:

"Cell volume regulation determines cell stiffness and gene expression patterning", Ming Guo, Enhua H. Zhou, Angelo Mao, Praveen R. Arany, Dylan T. Burnette, Karen E. Kasza, Frederick C. Mackintosh, Jeffrey J. Fredberg, David J. Mooney, Jennifer Lippincott-Schwartz, David A. Weitz, to be submitted.

Large portions of Chapters 6 have appeared in the following paper:

"The equation of state of living cells", Ming Guo, F. C. MacKintosh, David A. Weitz, to be submitted

Acknowledgments

I thank Dave Weitz, my advisor, for his guidance and mentoring on my research, and help and suggestions on my personal life. His enthusiasm, physical intuition, and ability to approach complex problems with clarity and simplicity, have very much shaped the type scientist that I aspire to be. I am always impressed by his untiring curiosity, work ethic, and generosity. He has managed to bring together a remarkable group of people in his lab, fostering a dynamic, collaborative, and fun research environment. I enjoy a lot of the past years in Dave's lab. I feel very lucky to be here!

During these years, I got help from many previous and current lab members. I thank Karen Kasza, Amy Rowat, Allen Ehrlicher, Adrian Pegoraro, Yi-Chia Lin, Lolo Jawerth, Stefan MÄunster, Liza Morris, Mikkel Jensen, Helen Wu and Sarah Koster for being excellent co-workers in the biophysics section of the group. I thank Peter Lu, Rodrigo Guerra, Anderson Shum, and Tom Kodger for being excellent colleagues.

The work presented in this thesis is the result of a number of excellent collaborations. The insight provided by theorists, Fred MacKintosh, has been invaluable in gaining a deeper understanding of this work. On the experimental side, Jennifer Lippincott-Schwartz and Bob Goldman have been there from the beginning, helping me with providing cells and proteins, and motivating much of the work presented here. It was a pleasure working with them. I thank Paul Janmey and Jeff Fredberg for their help and for a number of very enlightening discussions. Especially, during the past years, I have been talking with Fred MacKintosh and Jennifer Lippincott-Schwartz regularly about science, research and life. I'm very grateful for their mentoring and the time they spend besides busy work. I thank Jennifer for letting me stay at her home during my visiting in her lab. Both Jennifer and Fred are my great mentors that encoverge me to keep working hard and keep the curiosity for science!

I am very grateful to John Hutchison who recommended me to Harvard and to Dave. I ran into John several days ago, and he said Dave also thanked him for

recommending me to his lab. John is an extremely generous person and a great scientist!

Finally, I thank my wife Fei Deng for her continuous support and understanding and for making my years here in Boston very happy ones. I thank my parents their love and support. I especially thank my mom and my wife for encouraging me to work hard and enjoy whatever it is that I choose to do.

Dedicated to my parents and my wife.

Chapter 1

Introduction

1.1 Structure of this thesis

This thesis contains three major parts, which are connected by a common goal of trying to understand the physical nature of cytoplasm:

- A study of the mechanical and dynamic properties of the cytoplasm, including direct measurement of cytoplasmic material property using optical tweezers, and visualization of intracellular dynamics by tracer particles. We further combine these two measurements and obtain a directly characterization of the cytoplasmic forces. We apply these methods to study cancer cells and cells without certain cytoskeletal component. (Chapter 3, 4)
- A study of the role of cell volume in cell mechanics and cell biology. We show that the volume of a cell changes upon the property of the extracellular environment; the change in cell volume directly induces change in the mechanical property of both cytoplasm and cell cortex. We further show that the change in cell volume is due to intracellular water influx/efflux, and this has significant impact on cell biology. (Chapter 5)
- A direct characterization of the equation of state of living cells. We show that a living cell, under osmotic compression, behaves as Van der Waals gas with a hard sphere correction; its volume is dominated by intracellular ions. (Chapter 6)

1.2 Introduction and Background

Cells are highly dynamic: they crawl, change shape, and divide. In many critical biological processes, cells both exert and respond to forces in their surroundings; the mechanical properties of the cell are intimately related to this behavior. Cells also continually remodel their internal structure and thereby change their mechanical properties. An integrated understanding of cell structure and mechanics is thus essential for elucidating many fundamental aspects of their behavior, from motility to differentiation and development.

A variety of experimental techniques show that cells have both elastic and viscous characteristics, and thus are viscoelastic materials: their stiffness is similar to Jello, but they continue to slowly deform under a steady stress. Moreover, their elastic behavior depends on the mechanical properties of their environment.

When talking about cell mechanics, people normally refer to the mechanical properties of cell cortex, which consists a thick layer of crosslinked filamentous actin (F-actin) structure. The mechanical property of the cell cortex has been extensively measured by with variety of different techniques. However, as the major part of a cell body, the cytoplasm which consists most of key intracellular organelles provides the environment for cellular biochemistry other processes; therefore the mechanical properties of the cytoplasm is also crucial for understanding cells. However, due to experimental complexity, this has never been achieved before.

The mechanical properties of the cell and the cytoplasm are largely determined by the cytoskeleton, a biopolymer network consisting of three major components: F-actin, intermediate flaments, and microtubules. This knowledge lead to another approach to investigate the cytoplasmic property: in vitro studies of model networks designed to mimic the properties of the cytoskeleton [1, 2]. Great success has been achieved with this approach. However, the study with reconstituted network is still away from the real complicated cytoplasmic environment; a direct measurement in the cytoplasm of living cells is essential for us to understand the intracellular mechanics and how it

correlates with cell function.

Furthermore, bulk modulus which determines how much volume cells would change under pressure has never been directly quantified. Since bulk modulus is more relevant to many physiological processes, a quantitative measurement is essential. Quantification of bulk modulus is normally achieved by measuring volume of a system under a series of increasing pressure, which gives a measurement of the equation of state of the system. Moreover, the equation of state itself is also a fundamental identity for physical systems, and would certainly be fundamental for our understanding of the physics of living cells.

.

Chapter 2

Materials and Methods

2.1 Cell Culture, Microinjection, and Pharmacological Interventions

2.1.1 Cell Culture

Cells are maintained under 5% CO2 at 37°C in a humidified incubator. A7 cells [3] (gift from Tom Stossel lab at Harvard Medical School) are cultured in Dulbecco's minimal essential medium (DMEM) supplemented with 2% fetal calf serum, 8% newborn calf serum (Invitrogen), 10 mM HEPES buffer, 100 U/ml penicillin and 100 µg/ml streptomycin. WT and $Vim^{-/-}$ mEFs [4] are cultured in DMEM with 10% fetal calf serum, 5mM nonessential amino acids, 100 U/ml penicillin and 100 µg/ml streptomycin. MCF-10A cells are cultured in 1:1 DMEM:F12 media (Invitrogen) with 5% house serum (Invitrogen), 20 mM HEPEs, 10 µg/ml insulin, 0.1 µg/ml Cholera Toxin, 500 ng/ml hydrocortisone, 100 U/ml penicillin and 100 µg/ml streptomycin. MCF-7 cells and HeLa cells are cultured in DMEM with 10% fetal calf serum. Cells are plated on collagen I coated MatTek dishes at a density of 20 per mm^2 overnight before experiment.

2.1.2 Microinjection

Microinjection is performed using a glass needle and a FemtoJet microinjector (Eppendorf) mounted on a bright-field microscope. About 50 cells are injected per dish; each cell is injected up to 50 tracer particles to eliminate the interference to cell function. Cells are then allowed to recover in culture medium for 6 hours, and are imaged on a confocal microscope at 37 °C and 5% CO_2. Organelles and injected tracer particles are imaged with bright-field or confocal microscopy using a

63x/1.2NA water immersion lens on a Leica TSC SP5. Please refer to Extended Experimental Procedures for more details.

2.1.3 Pharmacological Interventions

To inhibit myosin II motor activity, blebbistatin (Toronto Research Chemicals) is dissolved in DMSO and added to cell culture media to a 10 μM final concentration, incubating for 30 minutes. ATP depletion is achieved by incubating cells with 2 mM NaN_3 and 10 mM deoxyglucose in PBS for 1 hour.

2.1.4 Osmotic Stress

Hyperosmotic stress is applied by adding polyethylene glycol 300 (PEG300) to isotonic culture medium. Cells are then allowed to equilibrate for 10 min at 37 °C and 5% CO_2, before we perform the imaging or optical-tweezer measurement. The cell size and mechanics equilibrate in 2 minutes after adding PEG based on our imaging and previous studies [5].

2.2 Fabrication of polyacrylamide gel substrate

Variably compliant polyacrylamide gels are made according to the procedure described by Pelham and Wang [6], on a 35 mm glass-bottom culture dishes (MatTek, Ashland, MA), with No. 1 coverslip on the bottom. Briefly, the glass is aminosilanized to activate polyacrylamide attachment. Gel stiffness is varied over 2 orders of magnitude by controlling the concentration of the cross-link bis-acrylamide (Bio-Rad, Hercules, CA) from 0.05% to 0.3% at acrylamide (Bio-Rad) concentrations of 5% and 7.5%; gels are mainly made of 7.5% acrylamide trying to maintain a similar surface chemistry, but gels with shear modulus of 100 Pa and 1200 Pa are made of 5% gels. The polymerizing gel is covered with a second unmodified coverslip and inverted to create a flat gel surface. For traction measurements, a small

volume of 500 nm red fluorescent latex particles (Invitrogen) is added to the solution to act as a marker of gel deformation. The solution is polymerized on the aminosilanized coverslip by the addition of ammonium persulfate and *n,n,n',n'*-tetramethylethylenediamine (TEMED). After polymerization is complete, the top coverslip is removed and collagen I (Vitrogen; Cohesion Tech, Palo Alto, CA) at 0.1 mg/mL in solution is chemically cross-linked to the gel surface using sulfo-SANPAH (Pierce Biotechnology, Rockford, IL) activation method. Collagen attachment and uniformity is confirmed using fluorescent collagen (Elastin Products, Owensville, MO). As we have shown before [7], comparison with known amounts of fluorescent collagen dried on aminosilanized coverslips allows calibration of the collagen surface density to be ~250–650 ng/cm^2 for the gels used in this study [8]. Gel thickness is controlled to be 70–100 μm and is confirmed by microscopy. The elastic shear modulus G' of macroscopic samples of the polyacrylamide gels is characterized in a rheometer (AR-G2; TA Instruments, New Castle, DE).

2.3 Particle Surface Chemistry

Fluorescent carboxylate-modified polystyrene spherical particles (100 nm, 200 nm and 500 nm, from Molecular Probes) are rendered inert by grafting short amine-terminated methoxy-poly(ethylene glycol) to the surface of carboxylated microspheres, as described previously [9]. PEG coated particles are stored at 4°C and used within two weeks. Both yellow-green and far red particles for each size are used in this study.

2.4 Particle Tracking and Analysis

The trajectories of the fluorescent particles are recorded every 10 ms for about 2 minutes. The images are processed with particle tracking software written by J. Crocker, D. Grier and E. Weeks, in IDL (http://www.physics.emory.edu/~weeks/idl/). Particle centers are found in each image with an accuracy of 22 nm. The MSD of the probe

particles is nearly constant in time at short time scales ($t \leq 0.1$ s), and is about an order of magnitude greater than the noise floor.

2.4.1 Tracking vesicle movements

To monitor intracellular movement, we track the motion of endogenous vesicles that bud off from cellular membranes. These refractive vesicles are visualized by bright-field microscopy using a 633-nm laser and a 63x/1.2NA water immersion lens on a Leica TSC SP5 microscope. To avoid cell-boundary effects, only vesicles located away from the thin lamellar region and the nucleus and greater than ~1 μm deep within the cell are analyzed. This selection of vesicles avoids any interactions with the mechanically distinct cell cortex and nucleus. The trajectories of the vesicles are recorded every 18 ms for 30 seconds. Vesicle centers are determined by calculating the centroid of the vesicle's brightness distributions in each image with an accuracy of 20 nm. Vesicle trajectories are tracked in order to calculate the time and ensemble-averaged mean-square displacement (MSD), $<\Delta r^2(\tau)>$, where $\Delta r(\tau) = r(t+\tau) - r(t)$.

2.5 Cell mechanics measurement

2.5.1 Cytoplasmic material properties measured using optical tweezers

To optically trap and manipulate 500 nm beads in the cytoplasm of mEFs, the beam from a variable-power Nd:YAG solid-state laser (4 W, 1064 nm; Spectra Physics, Mountain View, CA, USA) is steered through a series of Keplerian beam expanders to overfill the back aperture of a 100x 1.3 numerical aperture microscope objective (Nikon S-fluor; Nikon, Tokyo, Japan). To steer the beam and manipulate the trapped bead, two acousto-optic deflectors are used (NEOS Technologies, Melbourne, FL, USA). Using a custom-written Labview program (National Instruments, Austin, TX, USA), the acousto-optic deflectors are manipulated to control the beam in the plane of the microscope glass slide. For detection, the bead is centered on a high-resolution position detection quadrant detector (MBPS; Spectral Applied

Research, Richmond Hill, ON, Canada) and illuminated using brightfield illumination from a 75 W Xe lamp. The linear region of the detector is calibrated by trapping a bead identical to those used in the cells in water and moving it across the detector using the acousto-optic deflectors in known step sizes. The trap stiffness is calibrated from the mean-squared Brownian motion of a trapped bead in water at various laser power settings using the principle of energy equipartition as previously described [10].

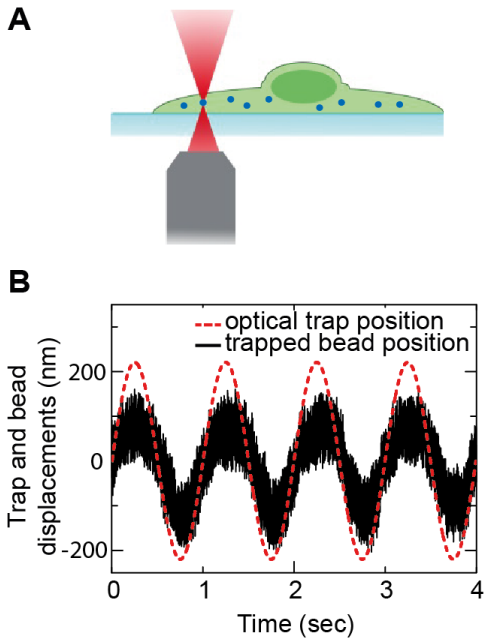

Figure 2.1. Optical tweezers measurement of intracellular mechanics. **(A)** Schematic of the optical tweezer experiment. 500-nm PEG coated inert particles are endocytosed into mEF cells, then trapped and manipulated by a spatially sinusoidal oscillating optical trap, which generates a force F at frequency ω. The frequency dependent complex spring constant is calculated by measuring the resultant displacement x of the bead in the trap oscillation, as F/x. **(B)** Typical displacements of the trapped bead and the optical trap oscillating at 1Hz.

Once calibrated, the laser trap is used to optically trap and manipulate beads intracellularly. The laser power at the sample is roughly 200 mW, corresponding to a trap stiffness of 0.05 pN/nm for the beads used Trapped beads are oscillated across a

frequency range of 1-100 Hz using the acousto-optic deflectors, and the laser position and bead displacement are recorded simultaneously, from which the elastic and viscous shear moduli are determined. By measuring the resultant displacement of the bead, $x(\omega)$, subjected to an applied sinusoidal trap oscillation with a force F at frequency ω, it is possible to extract the effective spring constant, $K(\omega)=F(\omega)/x(\omega)$, for a given intracellular environment. For materials with dissipation, the displacement, x, and force, f, are not in phase, which results in a complex spring constant. For a homogeneous, incompressible viscoelastic material, this spring constant is related to a complex modulus, $G=G'+iG''$, through a generalization of the Stokes relation $K=3\pi Gd$ *[11]*, where d is the bead diameter.

2.5.2 Cortical stiffness measurements

The mechanical properties of the cell cortex are probed using optical magnetic twisting cytometry (OMTC) which is a high-throughput tool for measuring adherent cell mechanics with high temporal and spatial resolution [12-14]. For these measurements, cells are plated on collagen I coated plastic dishes at a density of approximately 10 cells per mm^2 and allowed to grow overnight. 4.5-μm ferromagnetic beads (Integra Life Sciences) coated with poly-L-lysine (4 kDa) are incubated with the cells for 20 min to achieve strong coupling to the cell surface; poly-L-lysine binds to the cells nonspecifically and tightly, but does not induce active remodeling of the cytoskeleton [5]. Unbound beads are removed by gentle washing, leaving a few beads attached to each cell. The dish is mounted on a heated microscope stage to maintain 37 °C. Beads are magnetized by a strong, horizontal magnetic field and then twisted by an oscillatory vertical magnetic field at frequencies of f = 0.1 to 1000 Hz and amplitudes of about 25–50 Gauss. The motions of hundreds of beads in a field of view are recorded with a CCD camera (Hamamatsu C4742-95-12ERG) mounted on an inverted microscope (Leica DM IRE2) with a 10X objective, and the beads' positions are determined in real time with better than 10 nm accuracy by means of an intensity-weighted center-of-mass algorithm. The ratio between the torque and bead

motion thus defines an apparent stiffness for a cell, which has the unit Pa/nm. A series of geometric factors, based on finite element models that take into account the cell thickness and bead-cell coupling, can be used to convert the apparent stiffness into shear modulus of the cell, as discussed in Refs [12-14]. The bead-cell contact geometry is characterized by confocal fluorescence microscopy of labeled live cells; beads are embedded about 30% deep in WT and vimentin$^{-/-}$ mEFs (data not shown), so the same geometric factors are used. Previous measurements of cortical stiffness using OMTC agree with values obtained by other methods such as atomic force microscopy [15].

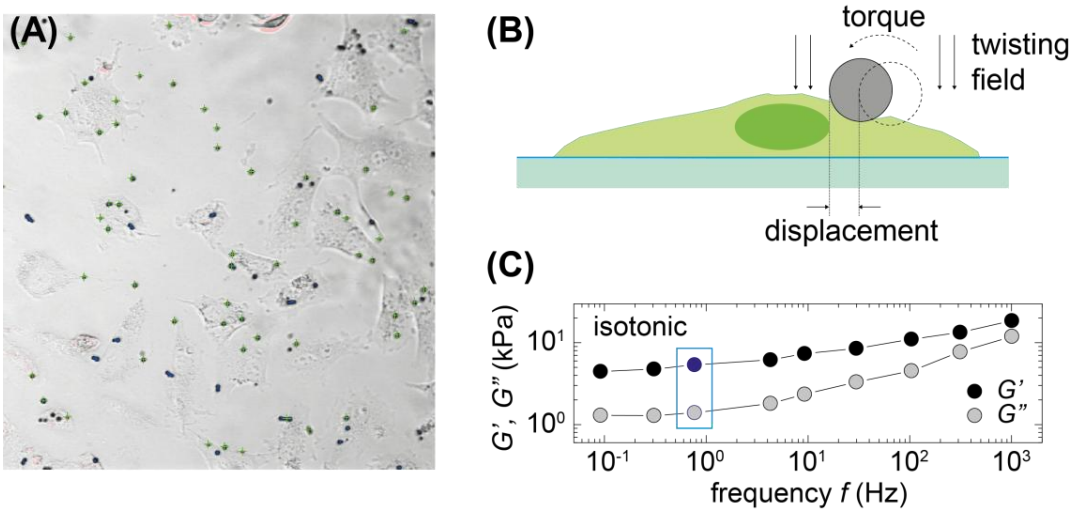

Figure 2.2. OMTC set up and power-law rheology of cell cortex. **(A)** A typical micrograph showing 4.5-μm magnetic beads adhered to individual A7 cells during an OMTC measurement. **(B)** Schematic illustration of the OMTC measurement. A magnetic field introduces a torque that causes the 4.5-μm ferromagnetic bead to rotate and to deform the cell cortex to which it is bound. **(C)** A representative measurement of A7 cell cortex mechanics in isotonic medium using OMTC. The cell cortex exhibits power-law rheology behavior across four orders of magnitude in frequency. A noticable plateau in both *G'* and *G"* also exists at low frequency. For convenience and consistency, we use cortex modulus measurement at 0.75 Hz (indicated by the blue box) across all different microenvironmental conditions.

2.6 Measurement of Protein Movement with Photoconvertable Dendra2

To measure the large length scale movement of small proteins, we use the photonically switchable fluorescent proteins Dendra2, a photoconvertible fluorescent protein which irreversibly switches from green (GFP-like) to red (RFP-like) when exposed to a brief flash of 405 nm light [16]. We transfect HeLa cells with Dendra2 (Evrogen), then perform fluorescence loss after photoconversion (FLAC) measurements as described previously [17]. In FLAC measurements using Dendra2, we start with the green fluorescence of unconverted Dendra2, which allows us to identify cells with high expression that are bright. We then flash the cell with a brief (~50 ms) flash of 405 light, while monitoring both the green and red fluorescence. A dip in the green fluorescence is observed, but a bright spot of red fluorescence in the pulsed region is clearly visible. By monitoring the increase of red fluorescence at different distances from the pulsed region, we can quantify the movement of the Dendra2 probe throughout the cell. Please refer to Extended Experimental Procedures for more details.

2.7 Immunoblotting and immunofluorescence

2.7.1 SDS-PAGE and Immunoblotting

SDS-PAGE and immunoblotting are performed as previously described [18]. Briefly, cells are grown in 100 mm culture dishes and lysed in Laemmli sample buffer. Proteins separated by SDS-PAGE were transferred onto nitrocellulose membranes (Whatman, Protran nitrocellulose membrane) and probed with the following antibodies: Mouse anti-vimentin 1:7000 (clone v9), mouse anti-alpha tubulin 1:6000 (Sigma, St.Louis, MO) and mouse monoclonal anti-actin (clone c4, 1:8000) (Millipore, Billerica, MA). Peroxidase-conjugated goat anti-mouse (Jackson ImmunoResearch, West Grove, PA) was used at 1:10000 dilution. Blots were developed by SuperSignal West Pico Chemi-luminescent Substrate (Thermo scientific

Rockford, IL). X-ray films were used to image the chemi-luminiscence signals.

2.7.2 Immunofluorescence, microscopy and image processing

Immunofluorescence and microscopy are carried out as previously described [19]. Briefly, cells are plated on glass coverslips, grown overnight and fixed in ice cold methanol. The fixed cells are immunostained with chicken anti-vimentin primary antibody (Covance, Princeton, NJ) (1:400 dilution in PBS supplemented with 0.01% Tween 20 (PBST)) and Alexa 488 conjugated goat anti-chicken secondary antibody (Molecular probes, Invitrogen, Carlsbad, CA) (1:400 dilution in PBST). Nuclei are stained with Hoechst 33258 (Invitrogen, Carlsbad, CA). Fixed and stained cells are mounted on glass slides and imaged with a Zeiss Confocal LSM510 META microscope with oil immersion objective lenses (Plan-Apochromat, 63× and 100×, 1.40 NA; Carl Zeiss). Image processing is as previously described [20].

Chapter 3

The role of vimentin intermediate filaments in cortical and cytoplasmic mechanics

3.1 Abstract

The mechanical properties of a cell determine many aspects of its behavior; these mechanics are largely determined by the cytoskeleton. While the contribution of actin filaments and microtubules to the mechanics of cells has been investigated in great detail, relatively little is known about the contribution of the third major cytoskeletal component, intermediate filaments (IFs). To determine the role of vimentin IF (VIF) in modulating intracellular and cortical mechanics, studies are carried out with mouse embryonic fibroblasts (mEFs) derived from wild-type or vimentin$^{-/-}$ mice. The VIFs contribute little to cortical stiffness but are critical in regulating intracellular mechanics. Active microrheology measurements using optical tweezers in living cells reveal that the presence of VIFs doubles the value of the cytoplasmic shear modulus to approximately 10Pa. The higher levels of cytoplasmic stiffness appear to stabilize organelles in the cell, as measured by tracking endogenous vesicle movement. These studies show that VIFs both increase the mechanical integrity of cells and localize intracellular components.

3.2 Introduction

Cells are regulated by complex biochemistry, but are also inherently mechanical objects. The predominant elasticity of the cell arises from the cortex, which is the

stiffest part of cell. However, it is the cytoplasm that surrounds all the key organelles, and its mechanical properties are critical for a large number of cellular processes ranging from large-scale events such as maintenance of cell shape and generation of cell motility, to more localized events such as mechanotransduction, signaling, and gene regulation [21]. The cytoplasm is typically much less stiff than the cortex, although its mechanics have not been well quantified. In animal cells, the main contribution to cytoplasmic mechanics comes from the cytoskeleton, a scaffold that contains three major types of biopolymers: actin filaments, microtubules and intermediate filaments (IFs). Both actin filaments and microtubules are dynamic polymers that are essential for the movement of cells and force generation [22]. Their assembly is dependent on chemical energy derived from hydrolysis, and they polymerize in a polar fashion giving rise to highly dynamic structures that facilitate intracellular transport and cellular adaptation to changes in the external environment. In contrast, IF assembly is apolar and does not require the input of chemical energy from nucleoside triphosphate hydrolysis. The resulting filaments are generally considered to be more stable and mechanically robust than either actin filaments or microtubules [23-26].

Intermediate filaments are important for maintaining the shape of cells and nuclei, and for regulating cellular motility and adhesion, and more than 80 distinct human diseases are associated with mutations in IF proteins. Even single point mutations and deletions are manifest in severe diseases, including posterior cataracts [27], various muscle diseases [28], Alexander disease [29], blistering skin diseases [30] and neurodegenerative diseases [31, 32]. These diseases are usually related to incorrectly polymerized or organized IF structure, which in turn affects their network configuration in cellular architecture [33]. This suggests that the mechanical properties of the IF networks may be dramatically altered, in addition to possible changes in biochemical functionality. Recent *in vitro* experiments show that cytoplasmic vimentin IF can withstand significantly greater mechanical deformation than either microtubules or actin filaments [24], suggesting that vimentin may be a

critical component in the mechanical integrity of cells. *In vitro* study of IF networks has revealed details of how IF assembly and crosslinking by divalent cations gives rise to elastic network [34]. However, the contribution of IF to intracellular mechanics remains unknown.

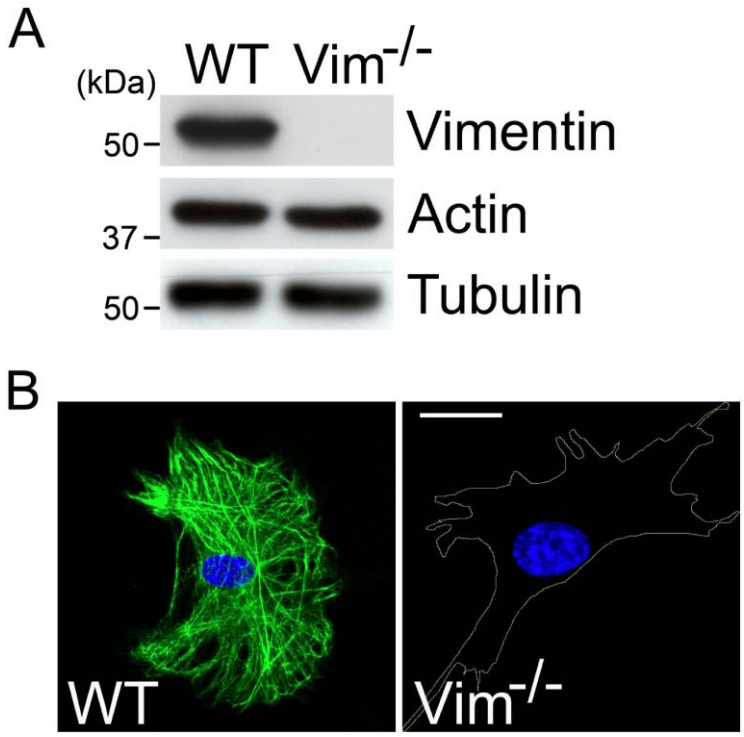

Figure 3.1. Analysis of control (WT) and vimentin$^{-/-}$ mouse embryonic fibroblast cells (mEFs). **(A)** Immunoblot analyses of cell lysates from WT and vimentin$^{-/-}$ mEFs using antibodies to vimentin, actin and tubulin. Representative blots from 3 experiments. **(B)** Immunofluorescence using antibodies against vimentin in control (left; WT) and vimentin$^{-/-}$ (right; Vim$^{-/-}$) mEFs. The cell boundary in vimentin$^{-/-}$ mEF is represented by the yellow line. Representative images from 3 experiments. Scale 10 μm.

In this paper we report the results of a direct measurement of the mechanical contribution of vimentin IFs to the cell cortex and internal cytoplasm. To quantify the effect of vimentin IFs, we use mouse embryonic fibroblasts (mEFs) from wild type (WT) and vimentin knockout (Vim$^{-/-}$) mice. We use optical tweezers to perform active microrheology to probe the internal cytoplasmic mechanics, and show that vimentin

IF increase the cytoplasmic stiffness by a factor of 2. The cytoplasmic stiffness is about 10 Pa in wild type mouse embryonic fibroblasts, whereas it is 5 Pa in the $Vim^{-/-}$ mEFs. To quantify the contribution of vimentin IF to cytoplasmic dynamics, we track the fluctuating intracellular movement of endogenous vesicles. We find that the presence of VIF reduces intracellular movement and localizes these organelles. Using Optical Magnetic Twisting Cytometry (OMTC) [12-14], we also directly measure the cortical stiffness in both cell types; interestingly, by contrast to its effect on cytoplasmic stiffness, vimentin IF do not significantly change cortical stiffness of the cell. These mechanical contributions highlight the role of vimentin IFs as a significant and important structural component of cytoplasm.

3.3 Results

3.3.1 Vimentin IFs stiffen the cytoplasm

To measure cytoplasmic mechanics, we perform active microrheology using optical tweezers on single polystyrene particles that have been endocytosed by WT or $vimentin^{-/-}$ mEFs and are randomly distributed within the cytoplasm. These 500-nm-diameter particles are covered with lipid layers during endocytosis and can thus be transported along microtubules, however, most of the time these particles display random movement. To focus on the contribution of vimentin IF to cytoplasmic mechanics, we only measure movement of particles located away from both the thin lamellar region and the nucleus; this avoids these mechanically distinct regions of the cell. About 8 hours after adding particles, a 1064-nm solid-state laser is used to trap a single bead and to generate a sinusoidally oscillating force F on the trapped particle (see Materials and Methods section). By measuring the displacement of the trapped particle, $x(\omega)$, resulting from the applied oscillating force at frequency ω, we extract the effective spring constant, $K(\omega)=F(\omega)/x(\omega)$, for the intracellular environment. For purely elastic materials, displacement and force are in phase; for materials with viscous dissipation, the displacement and force are not in phase. This enables us to

determine both the elastic spring constant, *G'*, and the viscous loss component, *G"*.

Our active microrheology measurements in the cytoplasm exhibit a displacement that is almost in phase with the oscillating force, as shown in Figure 3.2; thus, the micromechanical environment in the cytoplasm of mEF cells is predominantly elastic rather than viscous. Moreover, the measured elastic modulus *G'* is consistently larger than the loss modulus *G"* over the frequency range investigated, from 1 to 100 Hz; this shows that the cytoplasm of mEFs is an elastic gel instead of a viscous fluid, when measured on sub-micron length scales. Furthermore, both the elastic modulus *G'* and the loss modulus *G"* increase with frequency, following a power-law form, $|G(\omega)| \sim \omega^{\beta}$, with $\beta \approx 0.25$; this observation agrees with the power-law rheology observed previously for living cells and biopolymer networks [12, 35]. This value is also in agreement with that obtained when a cell is stretched between microplates (β ~0.2-0.3) [36] or is locally externally deformed at the cortex using either magnetic tweezers or atomic force microscopy (β~0.2) [12, 37].

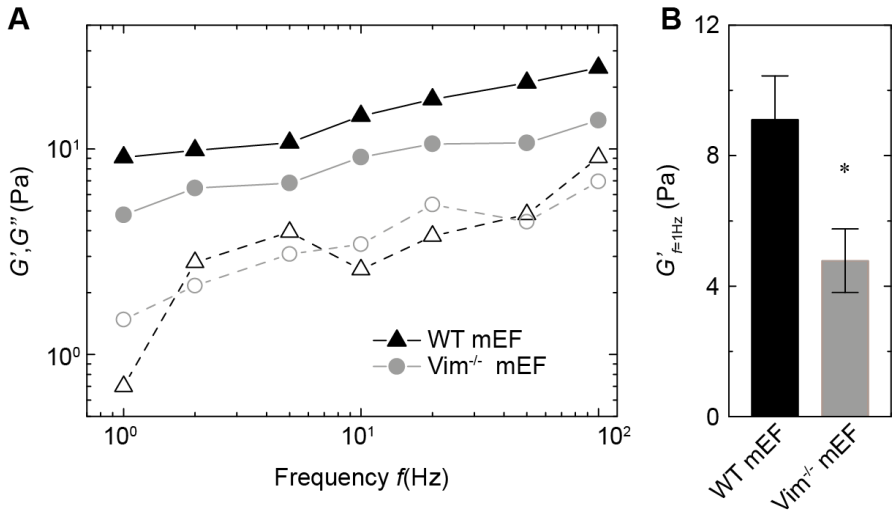

Figure 3.2. Active microrheology with optical tweezers controlling 500 nm endocytosed beads in the cytoplasm of mEFs. **(A)** Frequency dependent cytoplasmic elastic moduli *G'* (solid symbols) and loss moduli *G"* (open symbols) of the WT and Vim$^{-/-}$ mEFs. The cytoplasm of the WT mEFs (triangles) is stiffer than that of the Vim$^{-/-}$ mEFs (circles). **(B)** Cytoplasmic elastic moduli in the WT and Vim$^{-/-}$ mEFs at 1 Hz. Error bars, s.e.m (*P<0.05).

Although both WT and vimentin$^{-/-}$ mEFs show similar frequency-dependent behavior, the cytoplasmic elastic modulus, *G'*, of WT mEFs is larger than that of vimentin$^{-/-}$ mEFs, as shown in Fig. 3.2. Specifically, at 1 Hz the cytoplasm of WT mEFs is twice as stiff as that of vimentin$^{-/-}$ mEFs; thus the presence of vimentin increases the cytoplasmic elastic modulus from approximately 5 Pa to 9 Pa (Figure 3.2). However, the loss modulus *G"* is not significantly different between the WT and vimentin$^{-/-}$ cells over the investigated frequency range; the loss tangent, as defined by *G"/G'* which represents the relative dissipation of materials, is roughly twice as large for the vimentin$^{-/-}$ cells, indicating that the presence of vimentin also reduce energy dissipation in the cytoplasm. The significant difference in cytoplasmic moduli between WT and vimentin$^{-/-}$ mEFs reflects the contribution of vimentin IF to the intracellular stiffness, suggesting that vimentin is a crucial structural cellular component within the cytoplasm.

3.3.2 Vimentin IF reduces the intracellular fluctuating movement

The vimentin IFs also affect intracellular activity. To investigate how intracellular dynamics are influenced by cytoplasmic mechanics due to the vimentin IF network, we focus on the movement of endogenous vesicles, small organelles that bud off from cellular membranes to form sub-micron carriers that facilitate intracellular transport of materials. Bright-field microscopy is used to directly track the movement of such vesicles in wild type and vimentin$^{-/-}$ mEFs. We exclude trajectories from the thin actin-rich lamellar region and the mechanically distinct nucleus, focusing instead on the midplane of the cells where vimentin IFs are typically distributed. Occasionally, the motion is clearly directed, with vesicles moving along a straight path at a constant velocity, reflecting vectorial transport along microtubules by motors. However, the majority of the motion appears to be random, and the mean square displacement (MSD) increases linearly in time, reflecting the diffusive-like nature of the motion [38]. While the trajectories of vesicles in both WT and vimentin$^{-/-}$ mEFs indicate

random movements, the vesicles in vimentin$^{-/-}$ mEFs move further over the same time-scale, as shown in Figure 3.3. Quantifying the trajectories by plotting the MSD of these vesicles reveals that while both of them increase linearly with time, the vesicles move an order of magnitude faster in the vimentin$^{-/-}$ mEFs as compared to the control WT mEFs (Figure 3.3). Additionally, the slope of the MSD is slightly larger for the vimentin$^{-/-}$ cells (~1.27) than the WT cells (~1.21). This increased movement in vimentin$^{-/-}$ cells is consistent with previous observations of the movements of mitochondria [39], I melanosomes [40], the Golgi apparatus [41, 42] and other organelles [43, 44], suggesting that vimentin IF may contribute to determining the localization of a variety of different organelles.

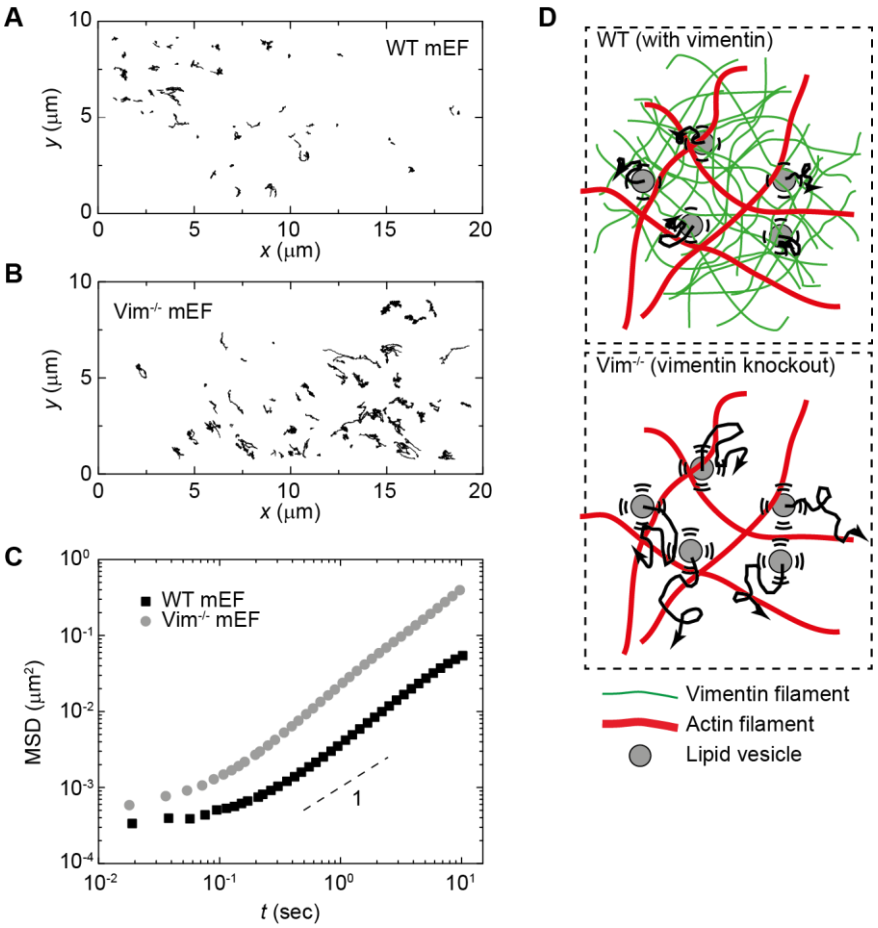

Figure 3.3. Intracellular movement of endogenous vesicles inside WT and Vim$^{-/-}$ mEFs. **(A,B)** 10 second trajectories of endogenous vesicles in the cytoplasm of (A) WT mEFs and (B) Vim$^{-/-}$ mEFs. **(C)** Calculation of the mean square displacement of vesicles shows that vesicles move faster in the Vim$^{-/-}$ mEFs as compared to the WT

mEFs. **(D)** Illustration of random vesicle movement in networks with and without vimentin. In the wild type cells, vimentin network constrains the diffusive-like movement of organelles; in the vimentin$^{-/-}$ cells, organelles move more freely.

3.3.3 Vimentin IFs do not change cortical stiffness

To determine if vimentin IFs contribute to the cell cortical stiffness, we measure the deformation of individual mEFs resulting from forces applied through a magnetic bead bound on the cell surface, a technique called OMTC (see diagram in Figure 3.4). This technique has been used extensively to measure material properties of cells [12, 14] and the results quantitatively agree with measurements obtained from other methods, such as AFM. The force-deformation relationship over 4 decades of frequency range is probed using OMTC, from which the elastic shear modulus, G', and the viscous loss component, G'', of the cell cortex are calculated (see Materials and Methods). The OMTC measurement reveals that the cell cortex of both WT and vimentin$^{-/-}$ mEFs are solid-like, with an elastic modulus G' much larger than the loss modulus G'' over the frequency range investigated, from 0.1 to 1000 Hz. The magnitude of shear moduli determined from the cortical OMTC measurements is two orders of magnitude larger than that of the cytoplasm. However, both G' and G'' of the cortex increase with frequency in a power-law form, as $|G(\omega)| \sim \omega^{\beta}$, with $\beta \approx 0.2$; both the power-law form and the value of β are in accord with the behavior of the cytoplasm, as well as with previous cortical measurements [12, 36, 37]. Interestingly, however, there is no significant difference in either G' and G'' between WT and vimentin$^{-/-}$ mEFs (Figure 3.4), suggesting that vimentin IFs do not affect the material properties of the cell cortex, which is mainly composed of actin filaments. Thus, these measurements highlight the specific structural role of vimentin IF in the cytoplasm rather than the cortex.

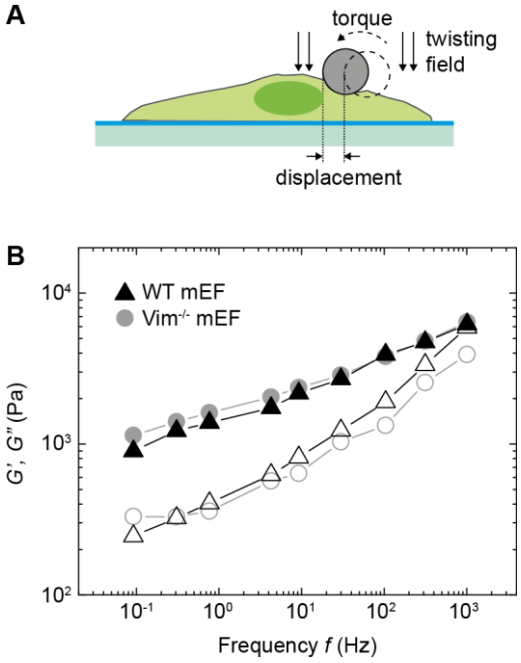

Figure 3.4. Cell cortical material properties of WT and vimentin$^{-/-}$ mEFs measured with optical magnetic twisting cytometry (OMTC). **(A)** Schematic of the OMTC measurement. A magnetic field introduces a torque that causes the 4.5-μm ferromagnetic bead to rotate and to deform the cell cortex to which it is bound. **(B)** Elastic, *G'* (closed symbol), and loss, *G''* (open symbol), moduli for WT (black triangles) and Vim$^{-/-}$ (gray circles) mEFs cultured overnight on Collagen I coated rigid plastic dishes, as measured by OMTC. About 100 single cells are measured for each cell type.

3.4 Discussion

Eukaryotic cells withstand a wide range of passive and active forces; they resist deformation, localize organelles and maintain shape under external forces. This mechanical robustness critically relies on the cytoskeleton, which is composed of filamentous polymers and regulatory proteins. The cell cortex forms a stiff shell that is mechanically dominated by a dense actin meshwork that together with myosin II creates a responsive and dynamic structure. Beneath the cortex, the cytoplasm is much softer, as it is composed of dilute structural proteins, organelles and cytosol. These two distinct cytoskeletal regions create a composite network that transmits mechanical signals from the extracellular matrix to the nucleus [17, 45], while

spatially organizing and mechanically protecting cellular components [46]. Therefore, cytoplasmic mechanics play a key role in many aspects of cell function, and mechanical defects may be directly related to pathology [47]. Intermediate filaments, as one of three major filamentous polymers of the cytoskeleton, are known to be involved in regulating cell movement, contraction, and internal transport [48-50], however, their role in the cytoplasmic mechanics has not yet been investigated. Our active microrheology measurements show that the cytoplasmic shear modulus of the WT mEF is about 80% larger than that of the vimentin$^{-/-}$ mEF. As compared to the WT mEF, the vimentin$^{-/-}$ mEF have the same amount of actin and tubulin, but no vimentin IF (Figure 3.1); therefore, the difference in our measurements reflects the specific mechanical contribution of vimentin IF. At 1 Hz, vimentin increases the cytoplasmic shear modulus from 5 Pa to 9 Pa (Figure 3.3). By comparison, *in vitro* rheology measurements of vimentin IF networks find an elastic shear modulus of a few Pa [35, 51]. In contrast, vimentin does not have any measureable effect on the cortical stiffness which is two orders of magnitude larger than the cytoplasmic stiffness (Figure 3.4). The substantially higher stiffness and the negligible contribution of vimentin in the cortex are both attributable to the dominance of the actin-rich structure of the cortex. Within the cytoplasm, actin network structures are less abundant, therefore vimentin plays a critical role in a variety of properties. In addition to mechanical changes, cells without vimentin IF have different shapes, lower motility and weaker adhesion [48-50]. Our results complement these findings by providing evidence that vimentin IF also contributes to the intracellular mechanics, suggesting that vimentin IF is essential for the structural integrity of cells.

In addition to contributing to cell mechanics, another major consequence of cytoplasmic vimentin IF is to spatially organize the contents of the cell [46]. Eukaryotic cells have a wide variety of organelles that serve different functions and these organelles distribute across the cell according to changing physiological needs and are in addition subjected to constant fluctuations due to thermal agitation and active forces [38]. By tracking the movement of sub-micron lipid vesicles, we show

that the vimentin IF network indeed reduces these random fluctuation of vesicles, in agreement with observations that the movement of other organelles, such as mitochondria, is confined by vimentin IF [39]. These results suggest that cytoplasmic vimentin IF, as a structural polymer, also helps to localize organelles in cells. This might be a direct consequence of the increase of cytoplasmic stiffness. Since vimentin IFs increase the cytoplasmic stiffness by about 80%, this reduces the random movement of contents that are integrated in the cytoplasmic network, and effectively localizes organelles, such as the nucleus and ER. This highlights how a structural biopolymer such as vimentin IF can have an extensive and unexpected impact through its mechanical properties.

Chapter 4

Probing the stochastic, motor-driven properties of the cytoplasm using force spectrum microscopy

4.1 Abstract

A living cell is a highly dynamic object, replete with active force generation due to molecular motors and other enzymatic activity. While motors often produce highly directed motion, the aggregate, incoherent effect of all active processes can create randomly fluctuating forces. These fluctuating forces can drive diffusive-like movements basic to many cellular processes. However, while these movements are diffusive-like, they are nevertheless distinct from movements arising from thermally-induced diffusive motion. There is no existing technique to measure the forces giving rise to these non-thermal based, diffusive-like movements inside cells. Therefore, understanding their characteristics has been challenging. Here we introduce Force-Spectrum Microscopy (FSM), a new assay that quantifies the random forces directly; it combines measurements of the random motion of probe particles with independent micromechanical measurements of the cytoplasm to quantitatively determine the spectrum of the force fluctuations. These fluctuating forces substantially enhance intracellular movement over a broad range of length scales. Moreover, the force spectrum is a sensitive assay that probes motor activity in cells. We demonstrate the utility of FSM by showing that force fluctuations are three times larger in malignant cancer cells than in their benign counterparts, consistent with the higher motility displayed by the cancer cells. In addition, vimentin-null cells exhibit enhanced motion of organelles as compared to wild type cells, despite the force spectrum being unchanged, implying that vimentin acts globally to anchor organelles

against randomly fluctuating forces in the cytoplasm. By appropriately interpreting random motion seen inside cells, FSM provides a means to extract important heretofore underappreciated consequences of the average random forces due to active motion in cells.

4.2 Introduction

The cytoplasm of living cells is not a static environment, but is instead subjected to a wide variety of forces [52]; for example, molecular motors such as kinesin and dynein generate forces that directionally transport cargo along microtubule tracks, while myosin II motors actively contract actin filaments [53]. These active processes all have clearly established functions in the cell, and their individual forces have been precisely quantified [53, 54]. Collectively, these forces have important consequences in the cytoplasm: Several motors operating coherently can generate large forces for directional transport [55, 56]. On an even larger scale, the cooperative activity of a large number of motors and other active processes collectively drive critical functions at the level of the whole cell, such as division, migration and contraction [57-61]. However, the aggregate effect of all the motors and active processes also contribute an incoherent background of fluctuating forces, and the ensemble aggregate of the forces from the incoherent effects of all cellular activities is directly associated with the functional efficiency and the overall metabolic state of the cell [57]. In the cytoplasm, these fluctuating forces can give rise, for instance, to random motion of vesicles, mitochondria and signaling proteins [62-68], and may drive an even broader range of intracellular dynamics. However, the random motion that arises from these forces is often interpreted as thermally-induced diffusion. It is, therefore, essential to have an assay that probes the ensemble aggregate forces due to overall cellular activity, as this could be a critical probe of the dynamic state of the cell, and may vary drastically with cell function or properties. Furthermore, a direct measurement of intracellular physical properties and forces is critical because these impact all intracellular

processes, and determine the dynamics of cytoplasmic components.

In this paper, we introduce force spectrum microscopy (FSM), an approach that probes the frequency-dependence of the aggregate, incoherent cytoplasmic forces within a cell. To accomplish this, we combine independent measurements of the intracellular fluctuating movement of injected particles with measurements of the mechanics of the cytoplasm performed with active microrheology using laser tweezers. With these measurements, we determine the temporal spectrum of the ensemble of the random, fluctuating forces. This confirms that fluctuating motion, so ubiquitous in cells, is not thermally induced, but is instead a consequence of these random forces. We then exploit FSM to probe the intracellular micromechanical behavior of malignant and benign cells, and show that cancer cells exhibit a significantly enhanced level of forces, albeit with the same frequency dependence, as predicted by our model. Moreover, we show that these active forces strongly dominate thermal Brownian forces in the cellular interior, impacting motion of objects from nanometers to microns in scale, providing a fundamental mechanism for transport of objects of all scales. Thus, FSM is a valuable new tool for characterizing the dynamic state of a cell.

4.3 Results and Discussion

4.3.1 Random intracellular movement appears diffusive

To measure the fluctuating motion in the cytoplasm of eukaryotic cells, we microinject sub-micron colloidal particles into A7 melanoma cells [3], and measure their time-dependent motion with confocal microscopy. The particles are rendered inert by attaching a short polyethylene-glycol (PEG) brush layer to their surface to eliminate interactions with biopolymers or proteins [9]; moreover, because they are microinjected, the particles are not surrounded by a lipid membrane. Furthermore, unlike smaller tracers that travel freely through the cytoskeletal network, these

sub-micron particles are larger than the typical cytoskeletal mesh size, which is about 50 nm (ref Luby-Phelps). Thus, their motion reflects the fluctuations of the cytoplasm itself. To avoid cell-boundary effects, we image particles that are greater than ~1 μm deep within the cell; we also image particles away from both the thin lamellar region and the nucleus to avoid any interactions with the mechanically distinct cell cortex and nucleus. Particle centers are determined in each image with an accuracy of 22 nm. We track their trajectories and calculate the time- and ensemble-averaged mean-square displacement (MSD), $\langle \Delta r^2(\tau) \rangle$, where $\Delta r(\tau) = r(t+\tau) - r(t)$. At shorter time scales ($t \leq 0.1\,\mathrm{s}$), the MSD of the probe particles is nearly constant in time; however, the fluctuations are always at least 5 times larger than the noise floor. At longer time scales ($t \geq 0.1\,\mathrm{s}$), the MSD increases approximately linearly with time, as shown in Figure 4.1. Particles of different size, *d*, exhibit a similar time dependence, as shown in Figure 4.1B. Moreover, the amplitude of the fluctuations scales as $1/d$, as shown in Figure 4.1C; this is consistent with motion in the continuum viscoelastic environment of the cytoplasm [38]. Such motion is often interpreted as thermal Brownian motion [64, 69-73]. However, a MSD that increases linearly with time is only consistent with Brownian motion in a purely viscous liquid and at thermal equilibrium, neither of which applies to the cytoplasm [68, 74, 75].

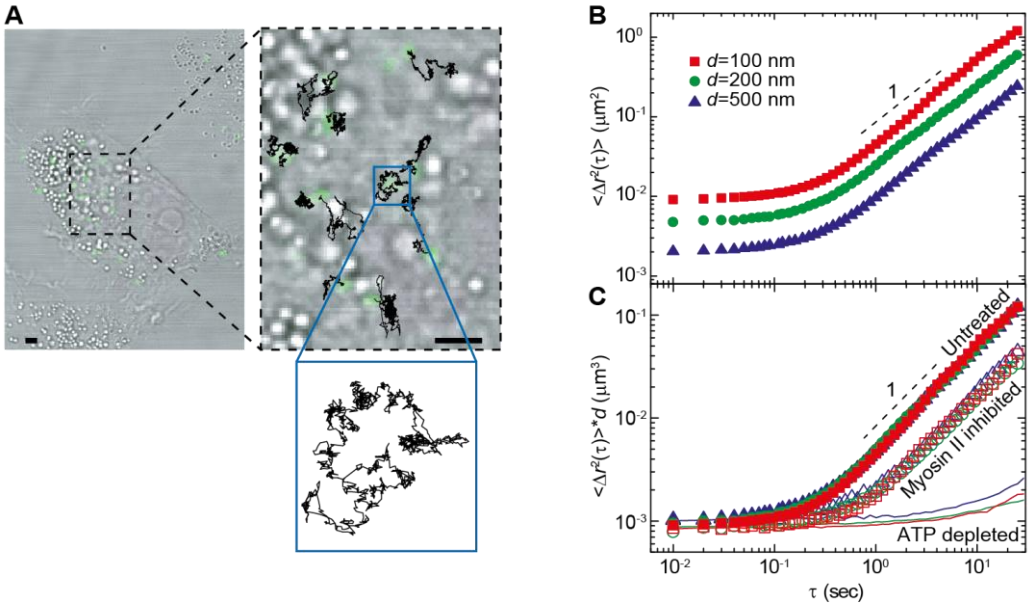

Figure 4.1. Movements of microinjected tracer particles in living cells. **(A)** Bright-field image of a A7 cell with microinjected 200-nm-diameter fluorescence particles (green) and two-minute trajectories (black) superimposed on top. PEG coated particles are microinjected into cells grown on collagen I coated glass-bottom dish. Particle trajectories in the cytoplasm look very similar with thermal Brownian motion. Scale bar, 5 μm. **(B)** Two dimensional ensemble-averaged mean-square displacement (MSD) $<\Delta r^2(\tau)>$ of PEG-coated tracer particles of various sizes are plotted against lag time on a log-log scale, in living A7 cells. Red, green and blue symbols and lines represent particles that are 100 nm, 200 nm and 500 nm in diameter, respectively. Dashed lines indicate a logarithmic slope of 1. Measurements are done with more than 200 tracer particles in about 25 individual cells for each particle size. **(C)** Ensemble-averaged MSD scaled with particle diameter, in untreated (solid symbols), blebbistatin treated (open symbols) and ATP-depleted (solid lines) A7 cells.

4.3.2 Cytoplasmic diffusive-like movement results from active processes

To demonstrate the active character of the cytoplasmic fluctuating motion, we explore the effects of motor activity on this random motion by treating cells with 10 μM blebbistatin, which inhibits myosin II motor activity. Myosin II is a nonprocessive motor protein that binds onto actin filaments and undergoes a power stroke upon ATP hydrolysis [52]. After inhibition, we observe a marked decrease in the MSD of injected particles in the diffusive-like regime ($t \geq 0.1\,\mathrm{s}$), while the shorter time-scale movement remains essentially unchanged. When we inhibit general motor and polymerization activity by depleting cells of ATP using 2 mM sodium azide and 10 mM 2-deoxyglucose, the MSD becomes nearly time independent over our experimental time scales (Figure 4.1C). Thus, the motion of the particles is driven by active, ATP-dependent processes. Such active behavior is not limited to the cytoplasm or to eukaryotic cells; ATP-dependent random fluctuating motion has also been observed in prokaryotic cells and yeast [76, 77].

To account for this behavior, we adapt recent theoretical work suggesting that diffusive motion in the cytoskeleton can arise from random motor activity [38, 78]: In

a filamentous actin network, acto-myosin contractile forces exerted by myosin II motors can drive fluctuating deformations. These myosin motors do not act individually but form aggregates, or minifilaments, which bind to the actin network and act as "disordered muscle fibers", applying random contractile forces in the network [79]. These forces can result in random fluctuations of the network, similar to that observed in reconstituted networks [11, 80, 81]. However, the theoretical framework of actively-driven fluctuations requires a network to be nearly elastic, rather than viscous, to account for the diffusive-like motion observed for $t \geq 0.1\,\mathrm{s}$. Thus, a direct measure of the intracellular mechanics is essential to ascertain whether the observed particle motion is due to thermal or active effects [74].

4.3.3 The cytoplasm is a weak elastic solid

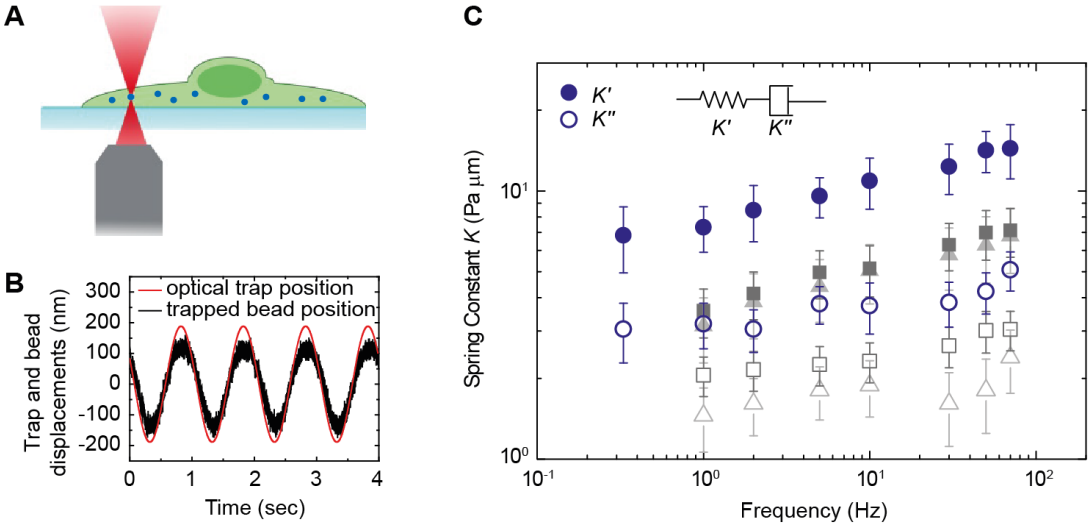

Figure 4.2. Optical-tweezer active microrheology measurement shows that the cytoplasm is a weak elastic gel. **(A)** Schematic shows the experimental setup used to measure the intracellular mechanics. **(B)** Typical displacements of the trapped bead and the optical trap oscillating at 1Hz. **(C)** Effective spring constant K_0 of the intracellular environment measured directly with active microrheology using optical tweezers shows that the intracellular elastic stiffness (solid symbols) dominates over the dissipative resistance (open symbols). Blue circles, grey squares, light grey triangles represent untreated, 10 mM blebbistatin treated, and ATP depleted A7 cells, respectively. Both the blebbistatin treatment and ATP depletion reduce the

cytoplasmic stiffness by about two folds. Error bars represent standard deviation (n=15).

To directly measure the micromechanical properties of the cytoplasm, we perform active microrheology measurements using optical tweezers to impose a sinusoidal oscillation as a function of frequency, υ, on a 500-nm-diameter probe particle within a cell. The trap stiffness is 0.05 pN/nm as determined using the equipartition theorem to describe Brownian motion of a bead trapped in water [10]. By measuring the resultant displacement of the bead, $x(\upsilon)$, subjected to an applied sinusoidal trap oscillation with a force F at frequency υ, we extract the effective spring constant, $K(\upsilon)=F(\upsilon)/x(\upsilon)$, for the intracellular environment [4, 11]. The complex shear modulus $G=G'+iG''$ is related to the spring constant through a generalization of the Stokes relation $K=3\pi Gd$. Thus, we can determine the full frequency-dependent modulus of the cytoplasm**.** Our active measurements yield a resultant displacement that is almost in phase with the applied force; therefore, the micromechanical response of A7 cells is predominantly elastic rather than viscous (Figure 4.2). Consistent with this, the measured elastic modulus G' is significantly larger than the loss modulus G'' over the frequency range from 0.3 to 70 Hz. The elastic modulus follows a power-law form, $|G(\upsilon)| \sim \upsilon^{\beta}$, with $\beta \approx 0.15$, in agreement with other measurements [4, 12]. We also note that the measured cytoplasmic modulus is approximately 1 Pa, much lower than that measured on the actin cortex [12]; presumably this reflects the denser cross-linked actin structure in the cell cortex, whereas the beads probe the cytoplasm which is much more dilute and hence lower in elasticity. Thus, our tweezers measurements confirm that the cytoplasm is an elastic solid, on the time scale measured.

4.3.4 Model of diffusive-like motion in a nearly elastic medium

The diffusive-like motion that we observe can be fully accounted for by acto-myosin forces in a nearly elastic medium. This can be understood most easily by considering the cumulative effect of multiple, random contractile forces exerted by myosin motors in an elastic actin matrix: the effect of uncorrelated myosin

contractions that individually consist of the sequence of binding, force generation and, finally, unbinding, gives rise to a net mean-square change in the force $\langle \Delta f^2(t) \rangle$ on a probe particle that increases linearly in time, as for a random walk. While individual myosin motors in an actin network are incapable of persistent, directed motion, when they self-assemble into minifilaments they become processive and can give rise to coherent motion, and hence force generation, over an extended period, the *processivity* time, τ_p. In this case, such minifilaments have a finite duty ratio, as the tension upon unbinding is instantaneously released, as sketched by the time-evolution of the force, *f*(*t*), in the inset of Figure 4.6C. Such a step-like force corresponds to a power spectrum of force fluctuations that varies with frequency, ω, as ω^{-2}. More precisely, for multiple myosin contractions that are governed by Poisson-distributed processivity times, the frequency-dependent *active* force spectrum is of the form [38, 78]

$$\langle f_{act}^2(\omega) \rangle \propto \frac{1}{\omega^2 + 1/\tau_p^2}. \tag{4.1}$$

For short times, $t < \tau_p$, this corresponds to $\langle \Delta f_{act}^2(t) \rangle \propto t$. At longer times, the finite processivity time limits the growth of $\langle \Delta f_{act}^2(t) \rangle$, as is also apparent from the fact that the right-hand side of Eq. (4.1) is finite as $\omega \to 0$. In a purely elastic medium, where displacement directly follows force, this accounts for diffusive-like motion, with $\langle \Delta x^2(t) \rangle \propto t$.

However, from our laser-tweezer measurement of the elastic modulus (Figure 4.2), the local micromechanical environment experienced by the probe particles is not purely elastic, but is instead viscoelastic, with a frequency-dependent spring constant $K(\omega) \cong K_0(-i\omega)^{\beta}$. In this case, the frequency- and force-dependent displacement becomes $x(\omega) = K(\omega)^{-1} f(\omega)$, which results in a particle displacement power spectrum

$$\langle x^2(\omega) \rangle = |K(\omega)|^{-2} \langle f^2(\omega) \rangle. \tag{4.2}$$

For the active spectrum in Eq. (4.1), this reduces to $\left\langle x^2(\omega)\right\rangle \propto \omega^{-2(1+\beta)}$ for $\omega > 1/\tau_p$. Thus, for times less than the processivity time, the mean-square displacement is

$$\left\langle \Delta x^2(t)\right\rangle = \int_{-\infty}^{\infty}\left(1-e^{-i\omega t}\right)\left\langle x^2(\omega)\right\rangle \frac{d\omega}{2\pi} \propto \frac{1}{K_0^2}t^{1+2\beta} \quad , \tag{4.3}$$

where $\beta \approx 0.15$. For a purely elastic medium ($\beta \to 0$), the active forces $\left\langle \Delta f_{act}^2(t)\right\rangle \propto t$, result in $\left\langle \Delta x^2(t)\right\rangle \propto t$. In a viscoelastic medium, for which $\beta > 0$, the MSD is enhanced at long times due to the fluid-like relaxation of stress at long times. The behavior in Eq. (4.3) is in stark contrast to the thermal motion expected in such a viscoelastic environment,

$$\left\langle \Delta x^2(t)\right\rangle \propto \frac{kT}{K_0}t^{\beta}. \tag{4.4}$$

This reduces to ordinary Brownian motion as $\beta \to 1$, which corresponds to a simple, viscous liquid, where stresses due to a fixed strain vanish at long times, resulting in unbounded motion. For viscoelastic fluids, this long-time stress relaxation is suppressed, and so is the resultant displacement in Eq. (4.4). Ultimately, for nearly elastic systems ($\beta \to 0$), a fixed displacement is expected, reflecting a simple balance of thermal and elastic energies. Thus, thermal motion in our case ($\beta \approx 0.15$) would have a much weaker time dependence than active motion; moreover, its amplitude would be thermal in character, depending on T. By contrast, the actively-driven motion has a much more pronounced time dependence, and its amplitude is not thermal in character, but instead depends on the driving forces of the motors.

The behavior exhibits three distinct regimes of time or frequency. This can be seen by comparing the active force spectrum, Eq. (4.1), with that of thermal forces, $\left\langle f_{th}^2(\omega)\right\rangle \propto kTK_0\omega^{\beta-1}$. On the shortest time scales or highest frequencies, thermal forces will tend to dominate, since $\left\langle f_{th}^2(\omega)\right\rangle \propto \omega^{\beta-1} \cong \omega^{-0.85}$ exhibits a weaker decrease than $\left\langle f_{act}^2(\omega)\right\rangle \propto \omega^{-2}$. At lower frequencies or longer times, active forces will dominate. Here, the MSD should follow Eq. (4.3), until $t \geq \tau_p$, at which point

$\left\langle \Delta x^2(t) \right\rangle$ should saturate to a constant.

4.3.5 Force spectrum microscopy (FSM) probes ensemble aggregate intracellular forces

The fluctuating motion of the tracer particles is a direct readout of the average random fluctuations due to the aggregate motor activity in the cell. If both the particle motion and the cytoplasmic viscoelasticity are measured, the spectrum of the average fluctuating force due to these motors, which drives this motion, can be directly determined, through $\langle f^2(\upsilon)\rangle = |K(\upsilon)|^2\langle x^2(\upsilon)\rangle$. This provides a new assay that characterizes the frequency-dependent spectrum of the average force, which is due to the aggregate, yet random effects of all active processes in the cell. While these forces are inherently time-dependent, it is more convenient to describe their frequency-dependent spectrum. We call this new assay Force Spectrum Microscopy (FSM), as summarized schematically in Figure 4.3.

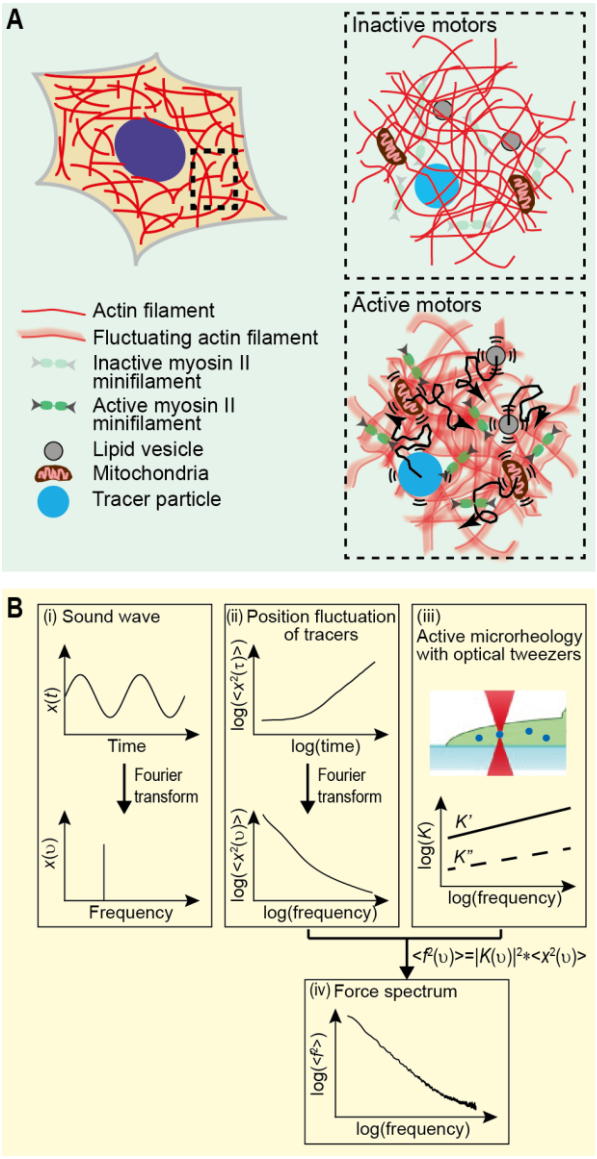

Figure 4.3. Conceptual basis of FSM. **(A)** Schematic illustration of cytoplasmic fluctuating forces enhancing intracellular movements. These active forces substantially enhance intracellular movement over a broad range of length scales, from sub-micron organelles to nanometer-sized proteins. **(B)** Basic procedure of FSM. (i) A sound wave in the time domain can be represented in the frequency domain by taking its Fourier transform, thereby revealing its frequency composition. (ii) By analogy to the sound wave, we Fourier transform the MSD and express it in the frequency domain. (iii) The cytoplasmic material property, specifically the spring constant, is measured directly using optical tweezers, also in the frequency domain. (iv) Analogous to a stretched spring, if the spring deformation and spring constant are known, the stretching force can be calculated; in cells, the randomly fluctuating force at each frequency is calculated as $\langle f^2(\upsilon)\rangle = |K(\upsilon)|^2\langle x^2(\upsilon)\rangle$.

To demonstrate the applicability of FSM, we quantify the average aggregate cytoplasmic forces due to active processes in A7 cells. The resultant force spectrum

exhibits two distinct frequency regimes, as shown by the red data in Figure 4.4A: In the low frequency range, corresponding to time scales $t \geq 0.1\,\mathrm{s}$, $\langle f^2(\upsilon)\rangle$ is proportional to υ^{-2}; by contrast, in the high-frequency range, corresponding to $t \leq 0.1\,\mathrm{s}$, $\langle f^2(\upsilon)\rangle$ has a weaker frequency dependency. These observations are consistent with a low frequency regime dominated by active forces, and a high frequency regime dominated by thermal forces [11, 38, 68, 78]. Moreover, based on our model, we estimate that a density of myosin filaments of ~1/μm^3, each generating a force of order 10 pN, can account for the observed force spectrum (see details in Supplementary Material). This is the only experimental probe of this important global measurement of the overall enzymatic activity in the cell.

To further establish the applicability of FSM in quantifying active forces in the cell, we suppress the level of the forces by inhibiting myosin II motors through the addition of 10 μM blebbistatin to the cell culture medium. As a result, the low-frequency, active component of the force spectrum is suppressed, although the same overall υ^{-2} dependence remains, as shown by the blue data in Figure 4.4A. Furthermore, when we deplete cells of ATP through addition of 2 mM sodium azide and 10 mM 2-deoxyglucose, we observe a force spectrum that is consistent with purely thermal fluctuations over the full frequency range for the viscoelasticy medium measured directly for these cells, as shown by the black data in Figure 4.4A. This suggests that, while actomyosin contractions are a significant source of intracellular forces, other enzymatic activities also contribute to the forces and hence the motion experienced by intracellular objects. Moreover, above 10 Hz, the force spectra measured in all cases have the same time dependence and nearly the same amplitudes, consistent with a common thermal origin of the motion in this regime (Figure 4.4A). These results demonstrate the ability of FSM to quantify the degree of motor activity in a cell, and to distinguish these active forces from thermal forces.

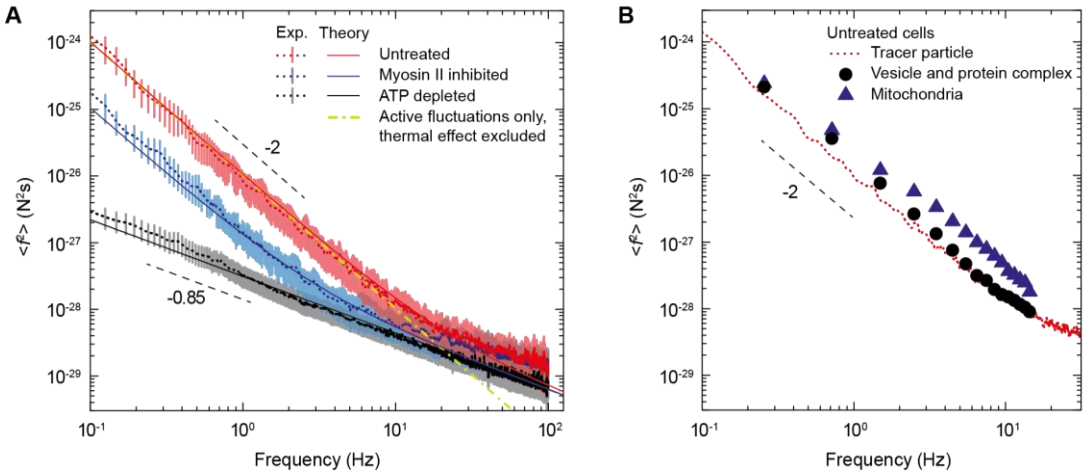

Figure 4.4. Ensemble aggregate intracellular force spectrum probed by FSM. **(A)** Cytoplasmic force spectrum calculated from spontaneous fluctuations of tracer particles and the active microrheology measurement, through $\langle f^2(\upsilon)\rangle = |K(\upsilon)|^2 \langle x^2(\upsilon)\rangle$, inside control untreated (red), myosin II inhibited (blue) and ATP-depleted (black) A7 cells. Data are shown as mean values (dotted lines) and vertical error bars (n>). For comparison, theoretical predictions are shown for an elastic medium with a shear modulus, with three levels of activities; the red solid line corresponds to about 1/ μm^3 density of myosin II filaments applying a force ~ pN, the blue solid line corresponds to a 90% reduction of myosin motor activity by 10 μM blebbistatin [82], and the black solid line corresponds to no active motors. The yellow dash dotted line represents the theoretical prediction of only active contributions and excludes thermal effects. Dashed lines indicate logarithmic slopes of -0.85 and -2. Vertical bars represent standard error (n=15). **(B)** Comparison of force spectra probed by FSM in untreated A7 cells, using the spontaneous fluctuations of injected tracer particles (red dotted line), endogenous vesicles and protein complexes (black circle) and mitochondria (blue triangle). The spring constant is measured by active microrheology with probe particles, as shown in Figure 4.2. The force spectrum measured with vesicles and protein complexes is in excellent accord with that measured for probe particles. The force spectrum for mitochondria exhibits the same frequency dependence as that for probe particles, but is larger in amplitude; this is consistent with mitochondria are also occasionally directly transported by specific motors within the cell.

To further explore the utility and sensitivity of FSM, we increase the cytoplasmic stiffness by applying osmotic stress to compress cells [5]. We observe a marked reduction in the amplitude of particle fluctuations, although the frequency dependence remains unchanged, reflecting the consequences of the increased cytoplasmic stiffness. Surprisingly, however, when the force spectrum is calculated, we find that the amplitude of intracellular forces does not change, at least within the range of osmotic

pressures applied.

4.3.6 Force spectrum microscopy probes the difference of intracellular forces in benign and malignant cells

Since FSM probes the consequences of the aggregate forces due to active processes in the cell, it can be used to directly quantify changes in intracellular activity and dynamic state of cytoplasm in response to changes in conditions such as drug treatment, external stimuli, or even the disease state of a cell. To illustrate this, we compare the force spectrum of malignant and benign cells. Malignant cells exhibit reduced cell stiffness [83, 84] and increased traction forces [85], which may provide potential biophysical markers for metastatic progression. Using FSM, we compare the force spectrum in benign (MCF-10A) to that in malignant (MCF-7) breast cancer cells which are known to exhibit enhanced motility [86, 87]. Tracer-particle motion is significantly enhanced in malignant MCF-7 cells relative to benign cells, as shown in Figure 4.5A, whereas the cytoplasmic stiffness is only ~30% smaller in the malignant MCF-7 cells (Figure 4.5B). When we calculate the force spectrum, we indeed find a significant difference between malignant and benign cells, with malignant cells having a force spectrum with approximately 3 times larger magnitude than the benign cells; however, the frequency dependence of the spectra remains unchanged (Figure 4.5C). We observe similar behavior for another pair of malignant and benign cells, M6C and M28 [88]. These suggest that the more motile malignant cells have a more active cytoplasm; this is consistent with other biochemical studies, such as proliferation and metabolic rate [89, 90]. Therefore, FSM provides a tool to identify changes in aggregate intracellular forces and dynamic state of the cytoplasm, although it does not directly distinguish the origin of these changes.

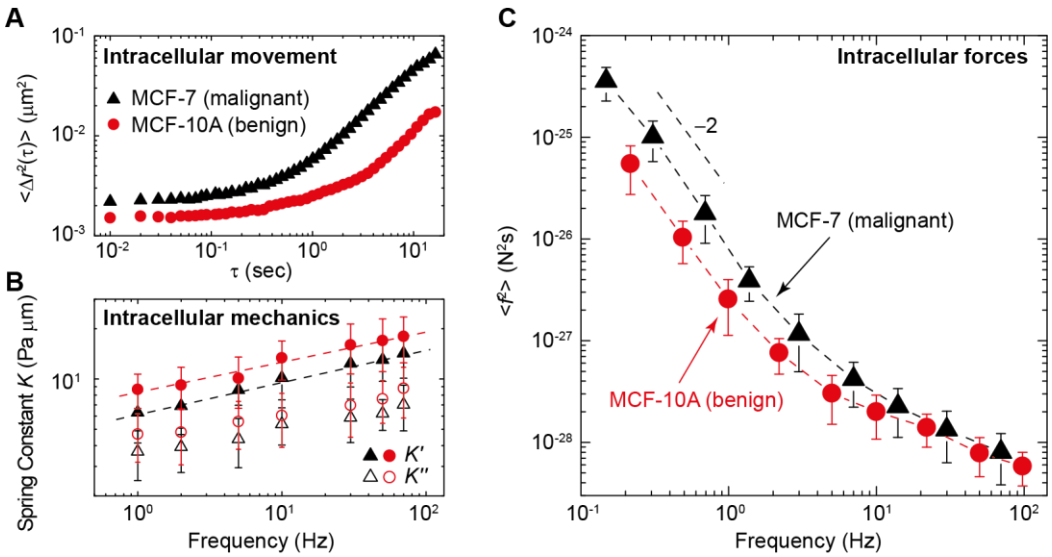

Figure 4.5. Intracellular mechanics, dynamics and forces in benign and malignant tumor cells. **(A)** Two dimensional MSD $<\Delta r^2(\tau)>$ of 500 nm tracer particles are plotted against lag time on a log-log scale, in the benign breast cells MCF-10A (red circle) and malignant breast tumor cells MCF-7 (black triangle), respectively. The fluctuating movement of tracer particles is stronger in the malignant cells, as compared to the benign cells. **(B)** Cytoplasmic mechanics measured by active microrheology using optical tweezers. The effective spring constant of the cytoplasm is larger in the MCF-10A (red circle), as compared to the MCF-7 (black triangle); this suggests that the cytoplasm of benign cells is stiffer than malignant cells. **(C)** The spectrum of intracellular forces calculated based on the fluctuating movement of tracer particles and the cytoplasmic mechanics measurement. The intracellular forces are stronger in the malignant tumor cells MCF-7 (black triangle), than the benign cells MCF-10A (red circle). Error bars represent standard deviation (n=6).

4.3.7 Force spectrum microscopy reveals that expression of vimentin intermediate filaments does not affect intracellular forces

Force spectrum microscopy can identify the contribution of specific cellular components to the overall level of intracellular activity. To demonstrate this, we apply FSM to measure the effect of vimentin intermediate filaments (VIFs) in mesenchymal cells. Vimentin is a type-III IF protein that is typically expressed in cells of mesenchymal origin and is widely used as a marker of the epithelial to mesenchymal transition (EMT). VIFs have been shown to induce changes in cell shape, motility and adhesion during EMT [48]; however, the role of VIFs in the level of aggregate intracellular forces is unknown because no technique has been able to quantify this

property. We use FSM to probe intracellular force spectrum in mouse embryonic fibroblasts (mEFs) from wild type (WT) and vimentin knockout ($Vim^{-/-}$) mice; we find no significant difference in the intracellular force spectrum between WT and $Vim^{-/-}$ mEFs. In contrast, the force spectrum is markedly reduced when we depolymerize actin filaments with 5 μg/mL Cytochalasin D in WT mEFs. These results suggest that vimentin IFs are mainly structural polymers that are an important contributor to the internal stiffness of cells, but do not affect the aggregate intracellular forces.

4.3.8 Force spectrum reveals motor processivity time

The frequency spectrum can quantify additional important, but heretofore unresolved, features of motor activity. This is seen in a more precise investigation of the time dependence of the MSD. At long times, $t \geq 0.1\,\mathrm{s}$, we observe an approximately linear time dependence in the MSD averaged over many particles. By contrast, our model predicts a stronger time dependence, as given by $\langle \Delta x^2(t) \rangle \propto t^{1+2\beta}/K_0^2$. This difference arises from the ensemble averaging over different trajectories; indeed when we examine the MSDs of individual particles, we find that most trajectories exhibit a markedly larger maximum local slope reflecting a stronger time dependence. However, they also exhibit clear evidence of a roll-off or saturation at the longest times, on the order of 10 s, as shown in Figure 4.6. This roll-off behavior is consistent with the finite processivity of motor contractions, at a processivity time, τ_p; processive forces are generated by motors with an average duration, τ_p, and result in finite displacements in the cytoplasm over corresponding **timescales**. To quantify this, we measure the distribution of logarithmic slopes of the MSD and find a peak near 1.2, as shown in Figure 4.6B; this is in excellent agreement with the prediction of $\langle \Delta x^2(t) \rangle \propto t^{1+2\beta}$ with $\beta \approx 0.15$. Moreover, the distribution of processivity times is peaked around 5 s, as shown in Figure 4.6C; this is the first experimental measure of processivity times for the ensemble aggregate forces. The processivity time is not apparent in the

ensemble average data, due to the large distribution in processivity times, τ_p, **obscures** the effect of individual turnover.

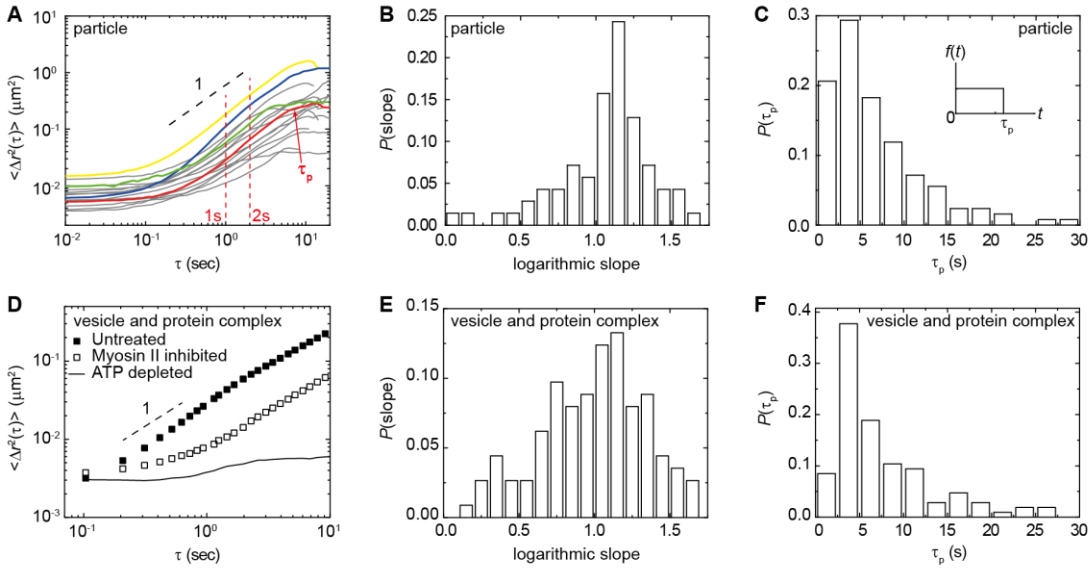

Figure 4.6. Logarithmic slope and processivity time analyzed from MSD of single tracer particles and cytoplasmic organelles. **(A)** Individual MSD curves of single 100-nm particles. Colored lines highlight representative deviations from the ensemble average. **(B)** Distribution of the average logarithmic slopes of single particle's MSD curve in untreated A7 cells, calculated between 1 to 2 second lag time as indicated by the red dashed lines in the inset. The mean and standard deviation of the slopes are 1.1 and 0.26, respectively, and the mode is about 1.2. **(C)** Distribution of processivity times τ_p associating with the random intracellular fluctuations, calculated from the transition between the diffusive-like regime and the long time saturation of the time-averaged MSD of each single particle, as pointed by a red arrow in (A). Inset, schematic of the time-dependent force due to activity of myosin filament. **(D)** Two dimensional MSD of the movement of intracellular vesicles and protein complexes, in untreated (solid squares) and blebbistatin treated (open squares) A7 cells, tracked by bright-field microscopy. **(E, F)** Logarithmic slopes (E) and distribution of processivity times (F) are calculated from MSD curves of single vesicle and protein complex in the untreated cells.

4.3.9 Active force fluctuations increase vesicle and organelle motion

Force spectrum microscopy provides a powerful assay to probe the consequences of the aggregate random forces due to motor activity within cells. In particular, it can be used to explore the consequences of these forces on motion of vesicles, protein

complexes and organelles within the cell, providing new insight into the origin of their random motion. . We use FSM to probe the effects of random forces on the overall movements of these various structures Motion of vesicles and protein complexes are tracked using bright-field microscopy in A7 cells. Occasionally, the movement is directed, with these structures moving along a straight path at a constant velocity; however, the majority of the motion is random in nature, with the MSD increasing approximately linearly in time (Figure 4.6D). We infer the force spectrum acting on thesevesicles and protein complexes using a combination of their MSD and the cytoplasmic mechanics measured with active microrheology using laser tweezers on tracer beads. We find that the force spectrum is in excellent accord, both in magnitude and frequency dependence, with that measured for injected probe particles (Figure 4.4B). Moreover, when we suppress the random cytoplasmic force by inhibiting acto-myosin contraction with 10 μM blebbistatin, we observe a marked decrease in their movements in direct analogy to the behavior observed for probe particles (Figure 4.6D). These results show that the random aggregate motor forces within the cell act on endogenous cytoplasmic structures in the exact same fashion as they do on the probe particles. This illustrates the ubiquity of the effects of the active random forces, and suggests that they may also contribute to intracellular transport.

We also apply FSM to probe the movement of mitochondria within the cell. Interestingly, we observe a force spectrum that exhibits the same frequency dependence as that of the probe particles, but is larger in amplitude by about a factor of 2, as shown in Figure 4.4B. By carefully observing the shape of mitochondria over time, we identify significant changes in their local configuration. This has an effect of shifting the center of the mitochondria identified during the tracking, thereby adding to the fluctuations, and is likely to contribute to the additional amplitude of the force spectrum. Moreover, it is known that mitochondria are occasionally transported by specific motors along microtubules. Therefore, the observed movement includes contributions from both random force fluctuations and effects from mitochondria

specific motors; this is also consistent with larger amplitude of forces observed on mitochondria. Thus, FSM is also able to probe the consequences of shape changes of the objects induced by the random forces, and might also provide a way to distinguish the specific and non-specific effects of motor activity on certain organelles.

4.3.10 Active force fluctuations increase protein movement

The force spectra revealed by FSM show that active processes dominate the ensemble cytoplasmic forces at relatively low frequencies (Figure 4.4A), which corresponds to long time scales. In contrast to micron-sized organelles and particles, smaller objects such as nanometer-sized proteins that are smaller than typical cytoplasmic mesh size, are much more mobile, and the role of the random forces on individual proteins is unclear. To investigate this, we examine both short and long time-scale diffusive-like behavior of nm-sized proteins. To examine short time-scale behavior, we transfect HeLa cells with green fluorescent protein (GFP), and perform fluorescent correlation spectroscopy (FCS) to measure the local dynamics of GFP, over timescales of tens of μs. At this scale, we do not resolve significant differences in the apparent diffusion coefficient of GFP between untreated and ATP depleted cells, implying that the random active forces do not affect the motion of individual proteins on short time scales. Nevertheless, since many signaling proteins and even nutrients travel across larger parts of the cell, over time scales of seconds, this is likely to be affected by the active fluctuating forces at long time scales. To investigate this, we transfect HeLa cells with Dendra2, a 26-kDa fluorescent protein that switches from green GFP-like fluorescence to red RFP-like fluorescence when flashed with 405 nm light [16]. By tracking the RFP signal after local photoconversion, we visualize the Dendra2-protein movement throughout the cell; we observe a marked decrease of the spreading of the RFP signal in the ATP depleted cells as compared to the untreated cells (Figure 4.7A; Movie S3). This is confirmed by plotting the time-dependence of the fluorescence intensity profile of the proteins. In the presence of ATP, the profile

spreads more rapidly (Figure 4.7B) with the width of the profile exhibiting more rapid expansion with time (Figure 4.7C). This result confirms that active forces contribute to the large-scale transport of individual proteins, suggesting that even the transport of small molecules or nutrients can be enhanced by random active processes.

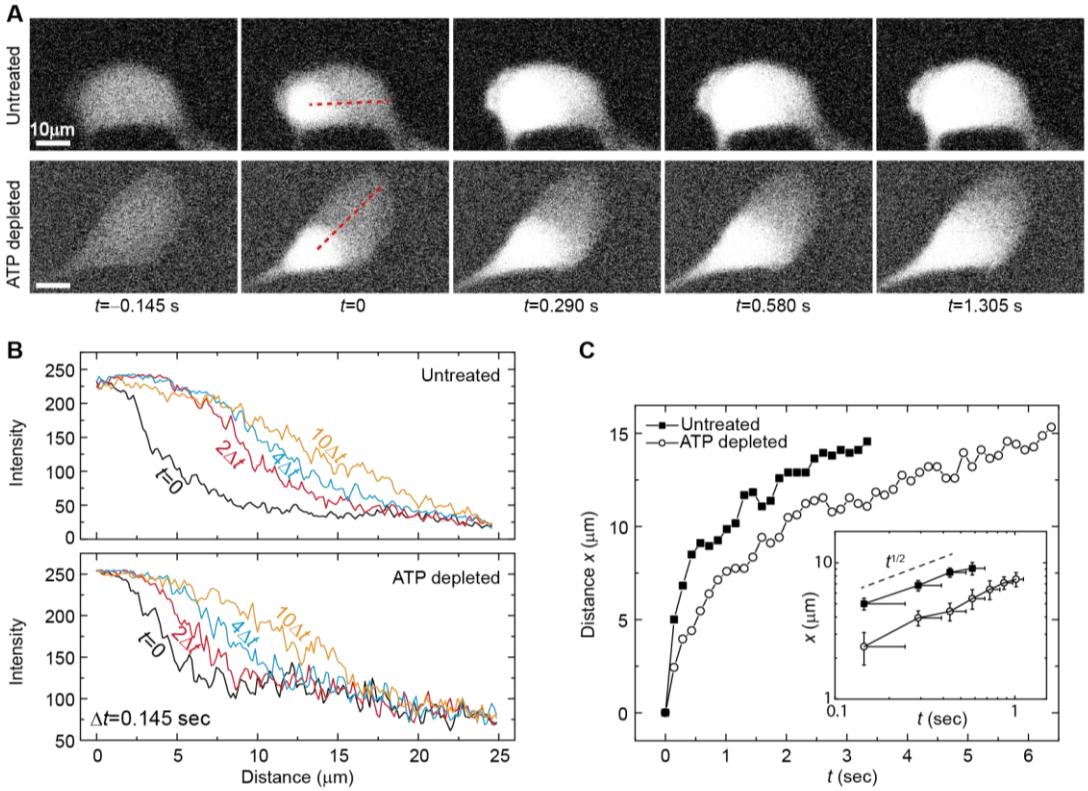

Figure 4.7. Movement of Dendra2 in cells is increased with ATP. **(A)** Typical confocal fluorescence images of the red-channel of Dendra2 during photoconversion by a 405 nm pulse. Before photoconversion, cells have low background red fluorescence; the flashed region rapidly converts to red, and begins to move throughout the cell over several seconds. Comparing the untreated and ATP depleted conditions, we see that red fluorescence spreads more quickly in cells with ATP. **(B)** By quantifying the red fluorescence intensity as a function distance (along the red dashed line in (A)) at several different times, we see that ATP approximately doubles Dendra2 transport over longer length scales. **(C)** Plotting the spatial width of the red fluorescence intensity as a function of time demonstrates that, without ATP, photoconverted Dendra2 spreads more slowly. **(Inset)** Replotting in log-log format shows that with or without ATP Dendra2 spreads proportional to $t^{1/2}$, demonstrating that both cases movement appears random. Error bars, 145 ms (based on measurement uncertainty from limited imaging frequency).

4.4 Summary and Outlook

We introduce a new assay, force spectrum microscopy (FSM) that directly quantifies the magnitude and frequency-dependence of the aggregate random active processes in the cell. We determine the force spectrum by tracking the random fluctuations of objects combined with the micromechanical characterization of the intracellular environment. This technique provides a direct measure of the forces within cells, which is very challenging by comparison to making the measurements of position or motion using microscopy. Furthermore, FSM provides the first direct measure of the random aggregate forces attributable to active processes inside the cell, and enables these to be distinguished from purely mechanical effects. This provides new insight into the consequences of the overall activity within the cell. Using FSM, we show that malignant cancer cells have significantly larger intracellular activity as compared to benign cells, demonstrating its utility in probing the internal dynamic state of cells. We confirm that vimentin IFs contribute mainly to structural mechanics, and not to the forces within the cell. We further show that FSM can be performed on intracellular organelles to investigate random forces experienced by organelles or different objects in cells. These results suggest that FSM may be used as a general assay to quantify the role of the random forces in driving many cellular processes.

Furthermore, our findings alter the way that we view the eukaryotic cytoplasm. Our results demonstrate that force fluctuations driven by motor activity play an important, even dominant role in intracellular motion over a broad range of length and time scales, from micron-sized organelles to nanometer-sized proteins and nutrients. These results also confirm that random motion, so ubiquitous in cells, is not a result of thermally-induced fluctuations, but is instead the result of the random forces due to the aggregate motor activity in cells. Thus, interpretation of intracellular motion based on equilibrium thermal fluctuations, such as is done for passive microrheology [64, 69-71] is incorrect. Moreover, this random motion driven by intracellular force fluctuations can have important consequences for many aspects of cell physiology.

For example, many cellular components, such as protein filaments and complexes, storage granules, and intracellular organelles, will be impacted by these active fluctuations in the cytoplasm; these components are involved in processes that are essential for life in natural environments, and their functions depends on their ability to move in the cytoplasm. More specifically, these random fluctuations are likely to be crucial for spatially distributing key cellular machineries, such as ribosomes and proteasomes, to facilitate efficient translation and degradation of proteins. They also could be vital for quick removal of enzyme products from their site of synthesis in metabolic reactions to avoid local concentration effects. Finally, growth and remodeling of the actin cytoskeleton may depend on these random force fluctuations, which may help ensure actin monomers are in continual supply to rapidly growing filaments in the cell periphery.

Chapter 5

Cell volume regulation determines cell stiffness and gene expression patterning

5.1 Abstract

Within a given microenvironment, how cells acquire and modulate shape stability can determine cell function and even influence stem cell fate. Here we identify an unexpected role of cell volume in these processes. As a cell spreads on a rigid substrate, the cell volume decreases as cell stiffness increases, and whether spreading on soft or rigid substrates, cell volume tracks cell spreading in an identical fashion. Moreover, changes in gene expression resulting from cell stiffening on rigid substrates could be replicated by altering cell volume by osmotic pressure. Taken together, these observations suggest that cell volume control through water release rather than through substrate rigidity underlies cell stiffness and downstream effects such as gene expression, and stem cell differentiation.

5.2 Introduction

Tissues within the human body span several orders of magnitude in stiffness: from soft tissues in the brain, to the stiff ones that constitute bone. This presumably reflects the behavior of single cells, whose stiffness appears to vary in response to the

mechanics of their surroundings: This has been shown by culturing cells on synthetic materials with controllable stiffness, such as polyacrylamide (PA) gels [6, 7, 91-93]. Cells grown on rigid gel substrates are markedly stiffer than those grown on soft ones [7, 92, 93]. Furthermore, this correlation between cell mechanics and substrate rigidity has been observed to influence stem cell fate [93-98]; naïve mesenchymal stem cells (MSCs) preferentially differentiate into neurons, myoblasts and osteoblasts on soft, intermediate and stiff PA gels respectively [93]. However, recent observations suggest that other physical factors can also affect cell stiffness; for example, cells grown on a substrate of uniform rigidity, but confined to adhesive patterns of varying size, exhibit changes in both their stiffness and shape [99]. Moreover, stem cell fate is affected by the pattern size as well [94, 100]. These surprising results suggest that the correlation between substrate rigidity and cell stiffness, while appealing, is incomplete. This correlation is essential to understand the cues that dictate stem-cell differentiation and that ultimately determine the development of the different tissues within the body. Thus further exploration of the relationship between cell mechanics and control parameters is essential.

In this paper, we present the results of a comprehensive study of the control parameters for cell stiffness. We show that, contrary to common expectations, cell stiffness is not determined by substrate stiffness; instead, cell stiffness correlates directly with cell volume. Cell area increases markedly with increasing substrate stiffness and the cells spread due to adhesion. However, cell height decreases with increasing spreading, and, surprisingly, cell volume also markedly decreases with

increasing substrate stiffness. However, when the spreading area of a cell is constrained the cell volume remains constant, independent of underlying substrate stiffness; moreover, the cell stiffness also does not change. Thus, cell stiffness is dictated by cell volume. In support of this, if cell volume is decreased through osmotic pressure, cell stiffness tracks the volume in exactly the same manner as when the volume is controlled by cell spreading. Remarkably, cell volume also affects stem-cell differentiation: When cell volume is decreased through osmotic stress on a soft substrate, mouse MSCs display precursor markers for osteogenic differentiation, which has been shown to be favored on stiff substrates and for large spreading areas.

5.3 Results and Discussion

5.3.1 Cell volume decreases with increasing substrate stiffness

To explore the parameters underlying cell stiffness, we examined how cell area, height and volume vary with the rigidity of the growth substrate. We reasoned that since cell stiffness changes according to substrate rigidity, then other cell parameters that similarly vary with substrate rigidity would be a candidate for having a role in cell stiffness control. A7 cells [3] were cultured on 100-μm-thick PA gels coated with collagen I. By varying bis-acrylamide crosslinker concentration, we tuned the elastic modulus of the gels from 0.3 to 30 kPa, matching the physiological elasticities of natural tissues [93]. To measure the different cell size parameters under the different substrate conditions, we labeled cells with CellTracker^{TM}, CellMask^{TM}, and DRAQ5^{TM} to label the cytoplasm, cell surface and nucleus, respectively.

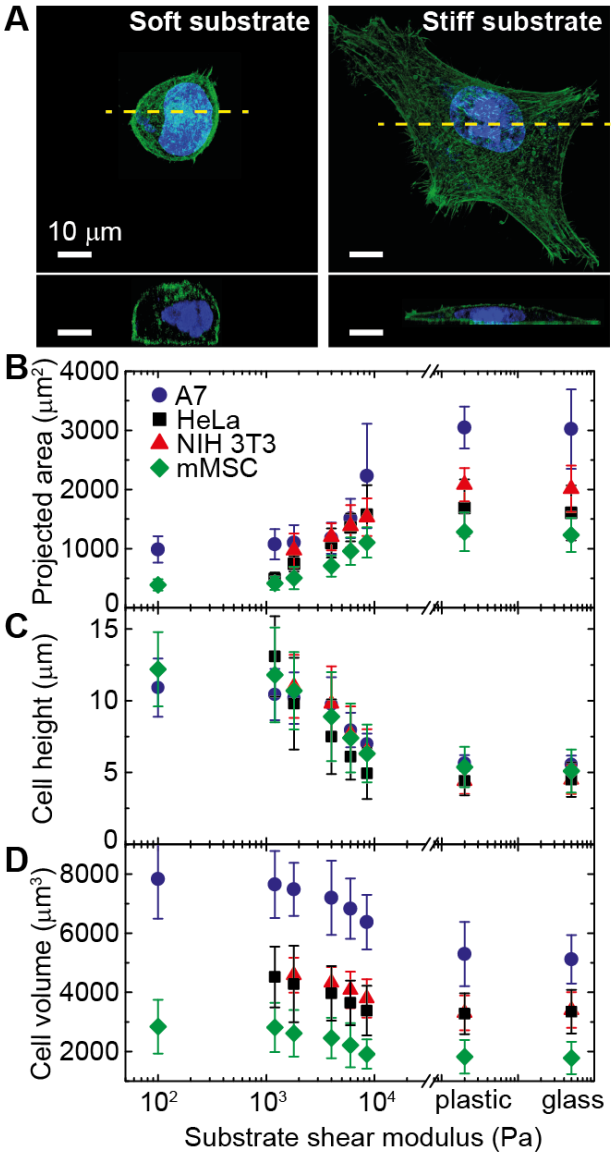

Figure 5.1. Morphology and volume of adherent cells change with increasing substrate stiffness. **(A)** 3 dimensional images of fixed A7 cells on stiff (shear modulus of 10 kPa) and soft (shear modulus of 1200 Pa) PA gel substrates coated with collagen I. Cells are fixed with formaldehyde, then labeled with Alexa Fluor 488 (green, Actin) and DRAQ-5 (red, nucleus). **(B)** The projected cell area increases with increasing substrate stiffness. **(C, D)** Cell center height (**C**) and cell volume (**D**) markedly decrease with increasing substrate stiffness. Error bars represent the standard deviation (n>200 individual cells).

Three-dimensional (3D) confocal microscopy imaging was then used to quantify the area, height, and volume of the cells. The measurement precision of each cell

shape parameter was verified by quantifying the size of fluorescently-labeled hydrogel spheres of diameters 10-30 μm; the results were within 8% of the values expected from the measured sphere diameter. Cell size measured on a stiff matrix by confocal microscopy was also compared to cell size measured by structured illumination microscopy (SIM). The comparison confirmed that our 3D confocal imaging approach was more than sufficient to make accurate measurements of different cell size parameters.

As the substrate became more rigid, cells increased their spread area (Figure 5.1A, B), as shown previously for many cell types [6, 7, 91, 92, 97]. The height of the cells, however, decreased dramatically on a rigid substrate, resulting in thinner cells (Figure 5.1C), but, surprisingly, cell volume was not conserved; as substrate rigidity increased overall cell volume decreased. On the most rigid substrates, cell volume decreased by as much as ~40% (Figure 5.1D). Other cell types, including HeLa, NIH 3T3 and mouse MSC, showed a similar volume decrease with growth on a more rigid substrate, indicating there is a generalizable relationship between cell volume and substrate rigidity.

5.3.2 Cell volume decreases with increasing cell spreading

We next tested if the decrease in cell volume during growth on more rigid substrates is specifically associated with the cell undergoing spreading. Cells were grown on a substrate of fixed rigidity but with the area of spreading restricted. This was accomplished by using micropatterned collagen islands of varying size that were

embedded on a glass substrate to limit the cell's adhesion area. We found that as the islands became smaller, and the capacity for cell spread area decreased, the cells rounded up and their volume increased (Figure 2A, B). This volume increase occurred even for cells grown on substrates with high rigidity (Figure 2B). Therefore, cell volume decrease during growth on more rigid substrates is dependent on the cell being able to undergo spreading.

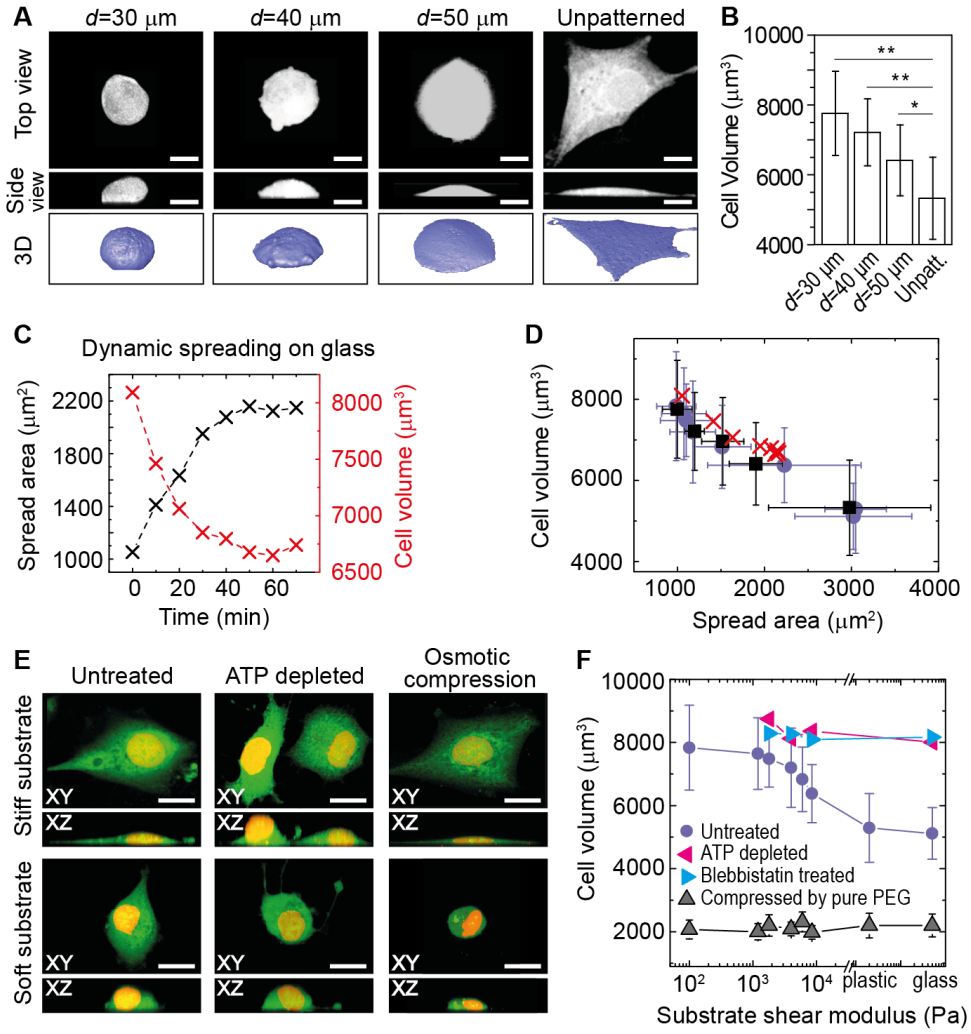

Figure 5.2. Cell volume increases when the cell spread area is decreased by growing cells on micropatterned collagen 'islands' on glass. **(A)** 3D images of cells on micropatterned island with different sizes on glass. Cells are labeled with CMFDA and imaged with confocal microscopy. Scale bars are 20 micron. **(B)** Bar plot of cell volume versus cell spreading area on glass. **(C)(D)** The relation of cell volume as a function of the projected area, for cells on substrates with different stiffnesses (blue

circles), cells on a glass substrate but with different available spread area (black squares), and a dynamically spreading cell (red crosses). **(E) (F)** Cells without active contraction (blebbistatin treated and ATP depleted) and under extreme osmotic compression do not exhibit a volume dependence with substrate stiffness. The control data of A7 cells is same as in Figure 5.1D. Error bars represent the standard deviation (n>200 individual cells, *P<0.05, **P<0.01).

To better investigate the relationship between cell volume and area of cell spreading, we also monitored a single trypsinized cell spreading on a coverslip. After placement of the cell on the coverslip, the cell spread out fully by 20 minutes. Throughout its spreading, the cell's volume decreased as the cell's spreading area increased (Figure 5.2C). Interestingly, the observed volume-to-spreading-area relationship was identical to that of cells grown on confined areas, as shown by the red × symbols in Figure 5.2D. Thus, spreading of a cell on a rigid substrate leads to a specific decrease in cell volume. This is distinctly different from the spreading of a drop of wetting liquid on a surface, where volume is always conserved.

5.3.3 Changes in intracellular water content

We next investigated the physical basis for the observed decrease in cell volume with increasing cell spreading. We reasoned that this behavior could result from either reduction of intracellular materials or water efflux out of cells. Reduction in intracellular molecular content typically takes hours for mammalian cells undergoing growth and remodeling [101]. By contrast, a significant amount of water can leave the cell within a minute [5, 102]. Since we found that cells rapidly decrease their cell volume during cell spreading on a glass substrate, the water efflux hypothesis seemed

more likely. Under this hypothesis, because water efflux would be mediating the cell volume decrease during cell spreading, no significant change in overall molecular content as the cell spreads is predicted. Therefore, the value of intracellular material and osmotically inactive water (i.e., water that binds molecular content) in the spread cells should be identical to that in cells that have not spread out. To test this prediction, we applied extreme osmotic pressure to cells by exchanging culture medium with pure, 300-Dalton polyethylene glycol (PEG), thereby extracting all free water from the cells. We then measured the resultant minimum volume, V_{min}, which roughly represents the amount of intracellular material and bound water that are osmotically inactive [5]. We found that V_{min} was independent of the substrate stiffness (Figure 5.2F), supporting the water efflux model prediction. We concluded, therefore, that the observed decrease in cell volume upon cell spreading was most likely a result of water efflux from cells.

We next asked how water might be extruded from spreading cells to cause their decreased volume. One possibility is through actomyosin contractility. It is known that actomyosin contraction is required for cell spreading [103]. Indeed, during mitosis, the instantaneous disruption of the actomyosin cortex causes cells to round up and increase volume [102]. To examine if the volume decrease upon cell spreading is due to enhanced actomyosin contraction, we treated cells with 10 μM blebbistatin to inhibit myosin II motor activity, which mediates contraction of the actin cytoskeleton. Notably, blebbistatin treatment prevented cells from decreasing their volume on stiff substrates. Instead, the cells exhibited similar 3D morphology and volume as those

grown on a soft substrate. The same effect was observed when we inhibited general motor activity by depleting ATP using 2 mM sodium azide and 10 mM 2-deoxyglucose (Figure 5.2E,F). Therefore, water efflux during cell spreading depends on actomyosin contractility.

5.3.4 Cell stiffness correlates with cell volume

We subsequently asked if cell volume reduction from water efflux during cell spreading is the primary factor underlying the increased cell stiffness known to occur during cell spreading. To address this, we measured cell stiffness after removing free water from cells by an alternative means to cell spreading; specifically, we employed osmotic pressure. By adding varying amounts of PEG to the culture medium [5], we found we could osmotically compress the volume of cells to different degrees and maintain this change for at least several hours without significantly affecting cell spreading, traction stress, and other substrate properties. This allowed us to adjust the cell volume independently from the other parameters that impact volume, including substrate rigidity and cell spread area. Cell stiffness was measured in these experiments by calculating the cortical shear modulus using optical magnetic twisting cytometry (OMTC) [5, 12]. This involved applying an oscillatory magnetic field at a frequency of 0.75 Hz and then using optical imaging to measure the force dependence of the deformation of a magnetic bead bound to the cell cortex.

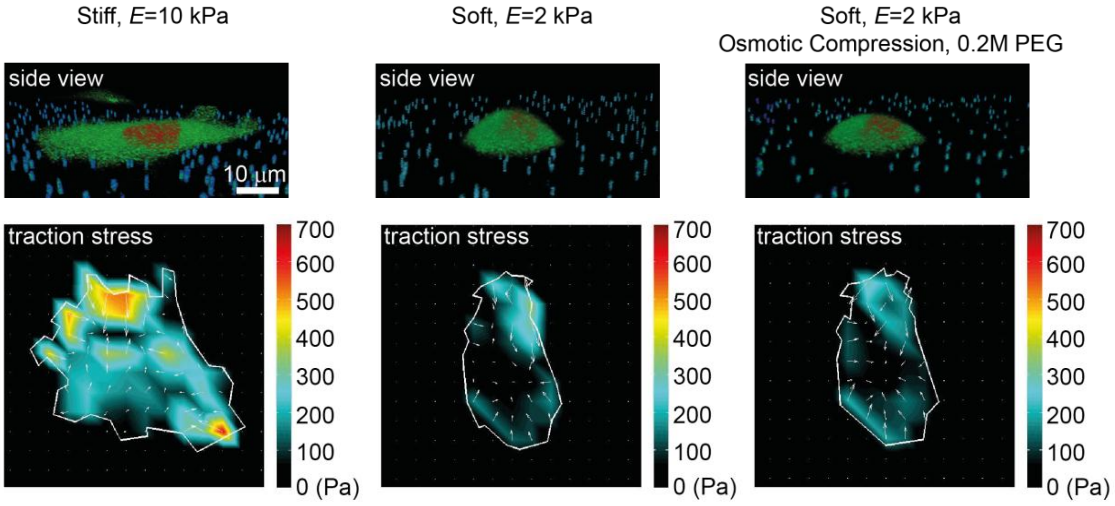

Figure 5.3. Cell morphology (top panel) and traction stress intensity map (bottom panel) of mMSCs on a stiff gel, a soft gel and a soft gel with osmotic compression. Mouse MSCs are cultured on a collagen I coated PA gel, with 500-nm fluorescent beads previously mixed in the gel substrate for visualizing traction displacement applied by cells. Cells on a stiff gel have larger spreading area and stronger traction stresses than those cultured on a soft gel. However, when we compress cells with osmotic pressure on a soft gel, while the height of the cell dramatically decreases, cell spreading area and traction stress does not change much. The cytoplasm and nucleus are labeled with cell tracker and DRAQ-5.

Using these approaches, we first measured cell stiffness under conditions of changing cell spreading and substrate rigidity. We found that the stiffness of freely spreading cells increased with substrate rigidity, as expected [92, 93] (see gray bars in Figure 5.3A). Surprisingly, however, the correlation between cell stiffness and substrate rigidity failed to occur when we prevented cell spreading through the use of micropatterned surfaces (Figure 5.3A). When cell spreading was prevented, no increase in cell stiffness occurred regardless of substrate rigidity; when the cell spread area was maintained constant through micropatterning, cell stiffness remained unchanged for all substrate rigidities (see black bars in Figure 5.3A). This suggested that substrate rigidity is not always a predictor of cell stiffness.

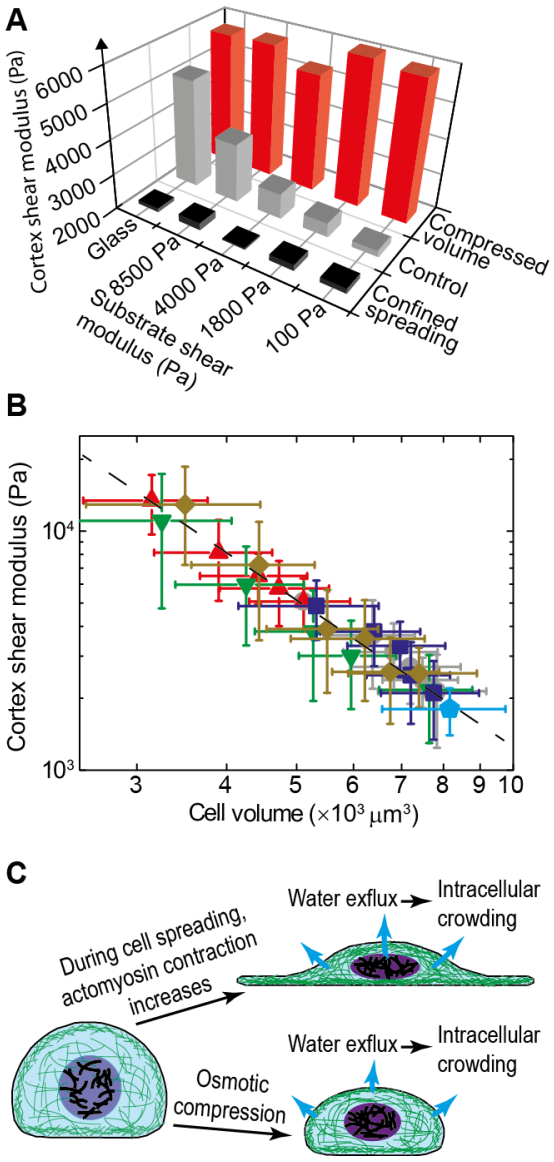

Figure 5.4. Cell stiffness correlates with cell volume. **(A)** Cell stiffness (represented by cortex shear modulus) of A7 cells grown on collagen coated PA gels increases with increasing substrate stiffness (control, grey bars). This is completely suppressed when cell spreading is prevented using small micropattened collagen 'islands' (black bars), or cells are compressed using proper osmotic pressures (red bars). **(B)** Cell stiffness scales with cell volume, as shown for cells growing on substrates of varying stiffness (grey circles, ●), on a glass substrate with different available spreading area using micropatterns (blue squares, ■), on a soft substrate (shear modulus of 100 Pa, green upside down triangles, ▼) with osmotic compression, on a unpatterned (red triangles, ▲) and a micropatterned glass substrate (yellow diamonds, ◆) with osmotic compression, and on a glass substrate with 10 μM blebbistatin treatment (cyan pentagon, ⬟ ,). Error bars represent standard deviation (n>100 individual cells). Dashed line shows the power-law fitting of the data, scales as V^{-2}. Error bars represent the standard deviation (n>200 individual cells). **(C)** Schematic illustration of cell

volume decrease through water exflux, due to increased actomyosin contraction or osmotic compression.

We then measured cell stiffness when cell volume was manipulated by osmotic compression. We found that when cells were osmotically compressed on a soft substrate, their stiffness increased immediately to match that of cells with the same volume grown on a rigid substrate. Moreover, when we osmotically adjusted cell volumes to be equal, cell stiffness remained unchanged as a function of substrate rigidity (see red bars in Figure 5.3A). The same behavior was observed when we compressed larger-volume cells grown on a micropatterned stiff substrate. Based on these results, we concluded that cell stiffness is not determined by substrate rigidity. Instead, cell stiffness correlates directly with cell volume.

To address whether cell volume control of cell stiffness requires actomyosin contractility, we treated cells with blebbistatin to inhibit myosin II activity. As the cells increased their volume under this treatment, we observed a corresponding decrease in cell stiffness. Therefore, actomyosin contractility underlies the relationship between cell volume and cell stiffness. This most likely occurs through a mechanism whereby actomyosin contraction leads to water efflux from the cell, making it both smaller and stiffer. Surprisingly, however, the osmotic stress required to affect a comparable volume change (~ MPa, as shown in table S1 and [5]) is much greater, by a factor of 100 to 1000, than expected cortical actomyosin stresses (~ 1 to 10 kPa, as shown in [103]). Moreover, the cortical shear moduli we observed suggest that the cortex cannot support such large osmotic stresses, implying that the volume

change is not due to purely mechanical expulsion of water. The above results suggested there could be an overall dependence of cell cortex stiffness on cell volume. To address this, we plotted the stiffness of cells whose volume is varied independently by controlling substrate rigidity, cell spread area, actomyosin contractility or osmotic pressure. Remarkably, the plot indicated cell stiffness is universally dependent on cell volume (Figure 5.3B), with the principle standing regardless of how cell volume or stiffness is adjusted.

The relationship between cell stiffness and cell volume could be a simple mechanical consequence of the effect of water release. As a cell shrinks through efflux of water, the fraction of intracellular material increases, and the stiffness increases concomitantly. Such behavior is commonly observed for composite materials, such as polymer composites and colloidal suspensions [104]. It has also been observed for cells under osmotic compression [5]. We wondered, therefore, if the stiffness increase observed in the cell cortex as the volume decreased could be related as well to the stiffness increase observed in reconstituted actin gels as the concentration, *c*, increases. The stiffness of these gels increases with concentration as $c^{2.2-2.5}$ [2, 105], consistent, within experimental uncertainty, with predictions of theory [106]. To test this, we fit the data in Figure 5.3B to a power law, and obtained a dependence of V^{-2}, as shown by the dashed line. Interestingly, this dependence is consistent with that observed and expected for reconstituted actin gels. This supports the idea that the relationship between cell stiffness and cell volume arises from water efflux, which increases the concentration of intracellular materials.

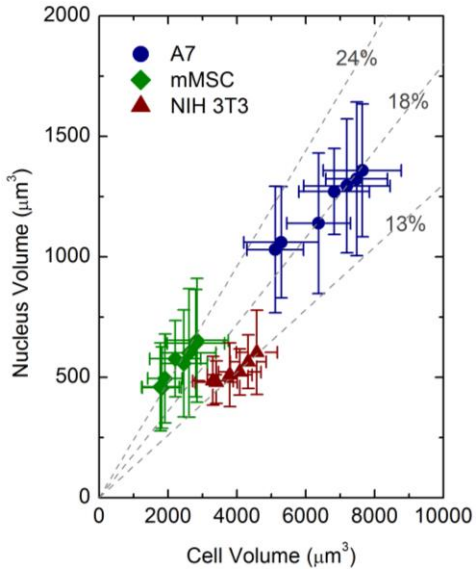

Figure 5.5. Cell nucleus volume tracks cell volume. Cells are grown on collagen coated PA gel substrates with different shear modulus, and glass. Cell nucleus is labeled with DRAQ5^{TM} and imaged in 3D using confocal microscopy. We observe that the nucleus volume directly tracks cell volume, decreasing proportionally with increasing substrate stiffness, spread area, and osmotic pressure. Error bars represent the standard deviation (n>200 individual cells).

5.3.5 Cell volume has impact on cell biology

If true, this would have major implications for understanding cell physiology and its control mechanisms. For most living species, the body water fraction is tightly controlled [107] and maintained within a certain range (from 50% to 70%) [108], which is important for many biological functions. The changes in the cell volume that we observed would also change the volume of intracellular water which would be expected to substantially change intracellular molecular crowding. This would undoubtedly cause significant variations in many internal physiological processes, such as protein folding and binding kinetics [109-111], structural rearrangement and molecular transport [5, 112, 113], and even gene and protein expression [107, 114,

115]. Moreover, these effects would also extend into the nucleus since we found that the volume of the cell nucleus decreased proportionally with cell volume (Figure 5.5).

Given the broad molecular consequences of a cell changing its volume and stiffness, we wondered whether differences in gene expression of stem cells differentiating on soft versus rigid substrates [93-98, 116, 117] could result from changes in cell volume and stiffness. That is, could the fate of differentiating stem cells be affected by changing cell volume and stiffness? To test this, we grew mouse MSCs on collagen coated PA gel substrates with two different stiffnesses: a stiff substrate with a shear modulus of 7 kPa and a soft substrate with a shear modulus of 0.2 kPa. We then exposed the cells to bipotential differentiation medium that is supportive of both osteogenic and adipogenic fates. To isolate the effect of cell volume from substrate properties, we applied additional osmotic pressure by adding 0.1M PEG-300 to the medium to compress the volume of cells on the soft gel to the same level as those grown on the stiff gel (Figure 5.6 D-F). After 1 week of culture, we observed substantial osteogenic differentiation on both the rigid substrate and soft substrate having additional osmotic pressure, as indicated by alkaline phosphatase (ALP) activity. By contrast, cells on the soft substrate without additional osmotic pressure did not express significant differentiation markers (Figure 5.6A, B). This was confirmed by western analysis of the expression of osteogenic biomarkers runt-related transcription factor 2 (RUNX2) and bone sialoprotein (BSP) after 3 days of culture, as shown in Figure 5.6C. The results thus suggested that we could control the fate of

differentiating stem cells by changing their volume and stiffness independently from effects by the growth substrate.

5.4 Summary and Outlook

In conclusion, our results suggest that volume and stiffness characteristics of cells vary inversely, with stiffness increasing as volume decreases. This inverse relationship results from changes in water content within cells. That is, as cells decrease their volume, they move water out and become stiffer. The reverse occurs when cells increase their volume. Inverse changes in volume and stiffness could be seen for cells grown on a rigid surface (which stimulates actomyosin contractility and water release) as well as those exposed to osmotic pressure (which drives water out of the cell). Under both treatments, cell volume decreased and cell stiffness increased. Because both treatments similarly altered the differentiation state of stem cells, changes in cell volume and stiffness characteristics of cells would seem to have significant cell biological consequences. Our data suggest this likely occurs through changes in intracellular free water levels and intracellular crowding, and is consistent with the increasing concentration of the network proteins making up the cytoskeleton.

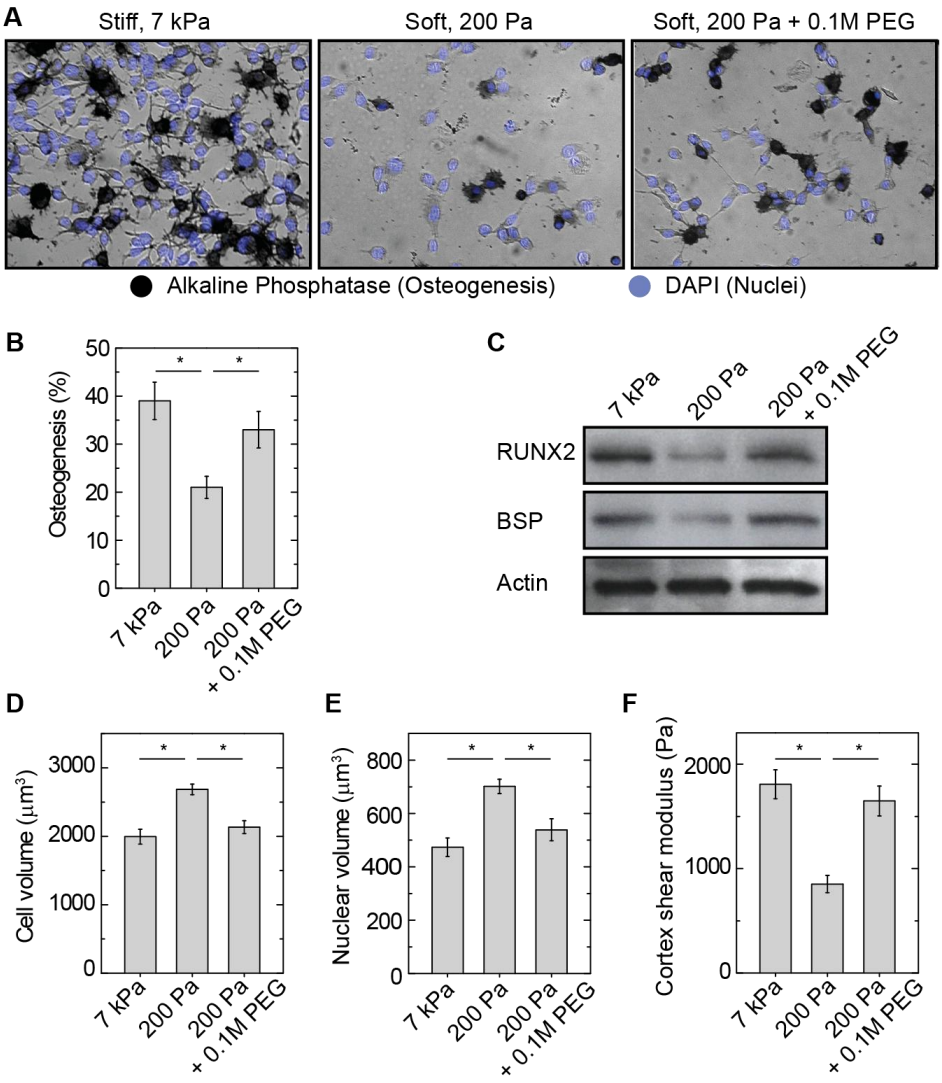

Figure 5.6. Differentiation of mouse mesenchymal stem cells (mMSC) is modulated by controlling cell volume. **(A)** In situ staining of mMSC for Alkaline Phosphatase (ALP, black) and nucleus (DAPI, blue) after 1 week of culture in the presence of combined osteogenic and adipogenic chemical supplements, show more osteogenesis on the stiff substrate (shear modulus of 7 kPa), and the soft substrate (shear modulus of 200 Pa) with osmotic compression (with 0.1M PEG-300 additionally to the medium). **(B)** Mean percentages of mMSC osteogenesis. Error bars, s.e.m (n=3, *P<0.05). **(C)** Western analysis of osteogenic protein expression (RUNX2 and BSP) in mMSCs after 3 days of culture. **(D-F)** Cell volume (**D**), nucleus volume (**E**) and cortex shear modulus (**F**) measured with confocal microscopy and OMTC, for 3 experimental conditions, (n>50 individual cells, *P<0.05).

Chapter 6

The equation of state of living cells

6.1 Abstract

In this chapter, we present a direct measurement of the equation of state of living mammalian cells. We find the *Π*-*V* relationship of cells can be described by a hard-sphere equation of state, corresponding to the Van der Waals gas without attractive interactions. Moreover, we find that the bulk modulus of cells is approximately three orders of magnitude larger than the shear modulus, suggesting that the cell cytoskeleton plays a negligible role in direct control of cellular response to osmotic stress.

6.2 Introduction

Cells are the basic unit of life and key to their survival is the ability to separate the cytoplasm from the exterior environment, both mechanically and chemically. This is done largely through the plasma membrane, but also via mechanical structures such as cell walls and interior cytoskeleton. These help cells withstand and respond to various stresses from their surroundings, including osmotic pressure. Both plant cells and many bacteria have rigid walls that can withstand a significant osmotic pressure differences between the interior and exterior of the cell. By contrast, the cell membrane of mammalian cells is mechanically much weaker and cannot withstand significant osmotic pressure differences; thus, the osmotic pressure within the cell must very nearly balance that outside the cell. Nevertheless, cell volume is known to

vary considerably during the life cycle of a cell, e.g., increasing significantly during cell division. In order to accomplish this, cells are believed to tightly regulate their volume by active control of ionic content, e.g., by ion-specific pumps. This can provide effective volume regulation because the plasma membrane is permeable to water, resulting in effective equilibration of internal and external osmotic pressure. Under these conditions, measurement of the cell volume as a function of externally applied osmotic pressure can be described by an effective equation of state for the cell. Moreover, from this equation of state, it would also be possible to determine the bulk, osmotic modulus of cell, which determines the resistance of the cell to volume changes. Measurement of these important quantities would provide considerable new insight into the properties of the cell: The bulk modulus would provide an excellent counterpoint to the shear modulus of mammalian cells, which has been extensively studied. Comparison between the two moduli would help determine the response to cells to changes in their mechanical surroundings, and would help resolve whether cells respond through changes in shape, while conserving their volume, or directly through changes in volume. Moreover, the equation of state would help elucidate the osmolarity of the cell, and hence the ionic concentration as well as the quantity of free water within the cell.

Here, we measure the equation of state relating osmotic pressure to volume of living mammalian cells, under both suspended and adherent conditions. We do this using confocal microscopy to measure the cell volume, which we control by osmotic pressure with the addition of polyethylene glycol to the cell medium. We determine the bulk (osmotic) modulus of the cells from their pressure-volume relationship. We find surprisingly good agreement in most cases with a hard-sphere equation of state, corresponding to the Van der Waals gas without attractive interactions, but with excluded volume only. To an excellent approximation, the cells' bulk moduli result from a passive gas of solute particles, likely dominated by intracellular ions. Surprisingly, cells seem to exert little control over their internal osmolarity. Rather, they respond primarily as passive bags of solute particles, over a wide range of

osmotic pressures, from isotonic conditions up to pressures as high as …. Only when cells are adhered to hard substrates, on which they spread considerably, do we find evidence of active regulation of intracellular osmolyte concentrations.

6.3 Results and Discussion

6.3.1 Relationship between cell volume and osmotic pressure

To measure the equation of state of living cells, and specifically the relationship between cell volume and external pressure, we grow cells in suspension and also on collagen coated substrates with different stiffness. We premix 300-Dalton polyethylene glycol (PEG) into isotonic cell culture medium to apply additional osmotic pressure. The relation between molarity and osmolality for solutions of PEG in water is taken from previous measurement (http://www.brocku.ca/researchers/peter_rand/osmotic/osfile.html). The actual osmotic pressure applied to cells is calculated by adding the osmotic pressure due to PEG to that of isotonic solution (300 mOsm); the pressure is selectively confirmed using a micro-osmometer. Cells are labeled with cell tracker to enable the volume quantification using confocal microscopy, as shown in Figure 6.1. After the addition of medium with PEG, cell volume suddenly decreases to an equilibrate value within 10 s, and maintains this steady state for at least 2 hours in our experiment, as shown in Figure 6.1. To confirm that cells achieve a steady state, we remove the additional osmotic pressure by exchanging back to isotonic medium, and find that cell volume returns back to its initial value instantly; as we cycle the osmotic pressure, cells always maintain at the same volume under a certain pressure (Figure 6.1).

Under increased applied osmotic pressure Π, the cell volume V decreases in a manner reminiscent of ideal gases: the volume varies approximately inversely with pressure, as shown in Figure 6.2 for cells in suspension. However, on closer inspection, we see clear evidence of excluded volume: the solid lines in Figure 2 show

$$\Pi = \frac{N k_B T}{V - V_{\min}}. \qquad (6.1)$$

This Hard-Sphere equation of state is similar to the van der Waals (VDW) model for gases, but without the attractive interactions. Here, the minimum volume is likely due to the intracellular protein and lipid content. The fit value of $V_{\min}$ is close to the cell volume we observe at the highest osmotic pressure of ~46 MPa. We observe excellent agreement with the equation of state (6.1) for a range of cell types in suspension, either trypsinized or naturally grown in suspension. We observe similar behavior for cells partially spread on soft substrates, as shown in Figure 6.2.

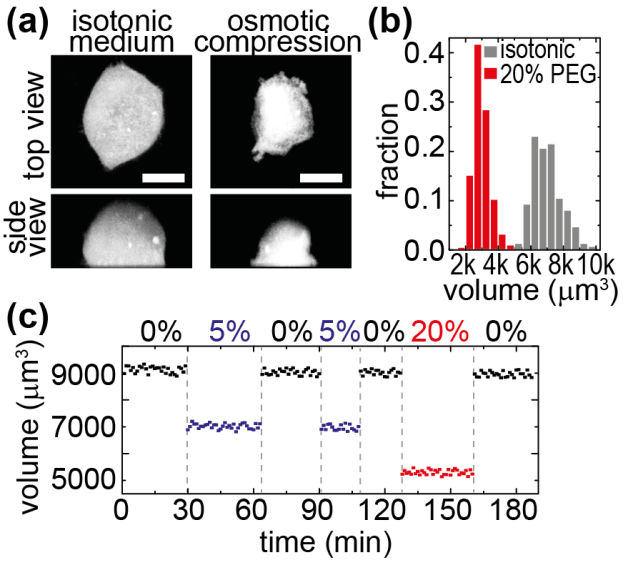

Figure 6.1. (A) Effect of osmotic pressure on adherent cell geometry measured using confocal microscopy. (B) Distribution of A7 cell size in isotonic medium, and under osmotic compression with 20% PEG. (C) cell volume decreases promptly with application of osmotic pressure, and maintains a static state until the pressure is changed again.

6.3.2 Intracellular ions dominate the equation of state of cells

The pressure in the Hard Sphere (or non-interacting Van der Waals) gas comes from the entropy of small, mobile particles. Here, we expect intracellular ions to dominate the entropy and the osmotic pressure. The number and concentration of these osmolytes can be obtained from Eq. (6.1) and Figure 6.2C. For both suspended cells and for all spreading conditions, we find a concentration of ~ 200 mM at high applied osmotic pressure. This is consistent with direct measurements of intracellular ion concentrations [21], consistent with the hypothesis that the *Π-V* relationship of

living cells is dominated by intracellular ions. Interestingly, for both suspended cells as well as those partially spreading on soft substrates (with a shear modulus of 1 kPa), our measurements are consistent with a total number of solute particles that remains constant over the full range of applied pressures, including isotonic conditions. Specifically, $\Pi \times (V - V_{min})$ exhibits no statistically significant variation over the full range of pressure for cells either in suspension or on soft substrates, as shown in Figure 2C. This suggests that the number of intracellular solute particles N remains surprisingly constant, in spite of the 3- to 4-fold change in cellular volume.

When cells spread on stiffer substrates, they are known to exhibit reduced volume. Near isotonic conditions, we observe a corresponding reduction in total intracellular solute number N, consistent with regulation to reduce pressure. We observe an approximate 25% reduction in N for cells spread on surfaces of intermediate stiffness (with a shear modulus of 6 kPa), and an approximate 50% reduction on hard surfaces (with a shear modulus of 20 kPa). This suggests that when cells spread and reduce their volume at low osmotic pressure, they actively expel or sequester intracellular solute particles. This can provide a mechanism for the cell to maintain low internal pressure, in spite of their reduced volume during spreading. Such active regulation could correspond to the more organized actomyosin cortex and the more active mechanotransduction system to sense external changes as cells spread out on stiff substrates. To explore this, we deplete cells of ATP using 2 mM sodium azide and 10 mM 2-deoxyglucose, then perform the compression measurement; ATP depletion stops cell's active response to external changes, such as ion pumps or transporters. As a result, we find the Π-V relationship recovers to Hard-Sphere equation of state (1), as shown in Figure 6.2. Interestingly, at high osmotic pressure, $\Pi \times (V - V_{min})$ converges to approximately the same value, independent of spreading conditions and ATP depletion, suggesting that the osmotic pressure overwhelms any active regulation of solute.

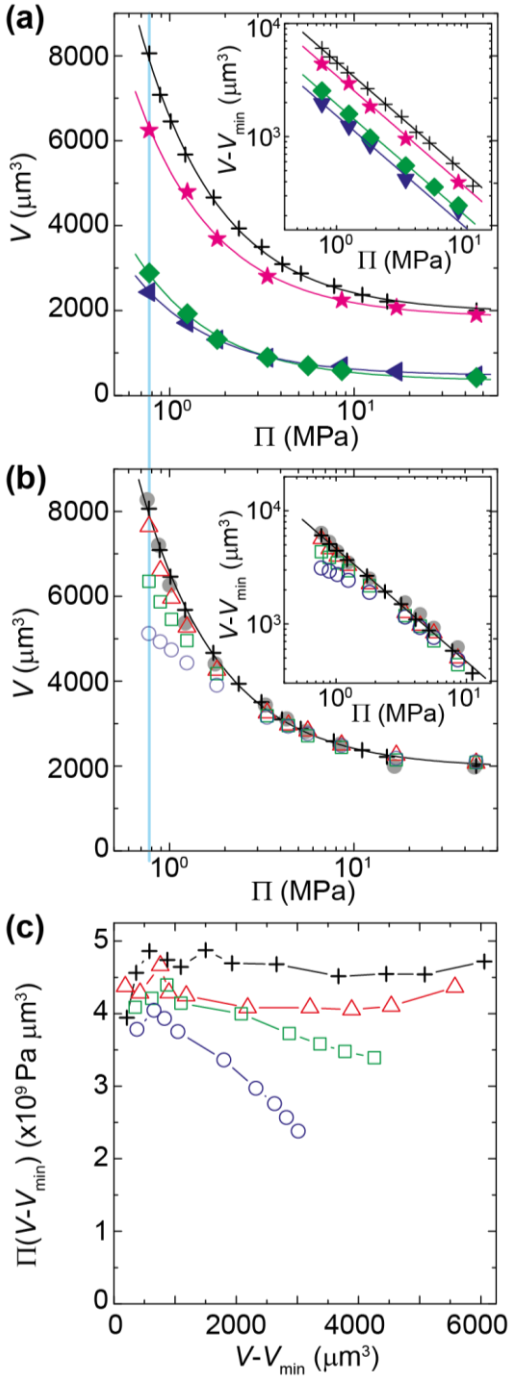

Figure 6.2 Dependence of cell volume on osmotic pressure of (A) several cell types in suspension, including , (B) A7 cells adhering on substrates with different stiffness. Solid lines represent fitting with equation (6.1). Insets: loglog plot of V-V_{min} versus osmotic pressure. (C) $\Pi\times$ (V-V_{min}) of A7 cells on substrates with different stiffness is plotted as a function of free volume V-V_{min}.

For the same cell type, the V_{min} is the same despite of spreading conditions,

consistent with the interpretation that cytoplasmic pressure is dominated by ions, while V_{min} is dominated by particles that are conserved during volume change. The volume we measure is consistent with rigid proteins with volume of a cubic nanometer, and a cellular concentration of ~ 1 mM [ref]. As this concentration is two orders of magnitude lower than *N* above, this provides us with another consistency check on the conclusion that the *Π*-*V* relationship is dominated by osmotic pressure of ions.

In general, the hard-sphere equation of state should be dominated by hard sphere interactions at high volume fractions. Indeed, although proteins usually have the ability to fold to achieve biological function, on monomer-scale, they are rather rigid to volume deformation. Such compliance might have led to a deviation from Eq. (1) at high osmotic pressures (small V-V_{min}), reflecting deviations from hard sphere behavior of proteins. However, we do not observe any evidence in our *Π*-*V* measurement for suspending cells within the pressure range we applied (Figure 6.2A). This might be because the number concentration of proteins is substantially lower than that of ions, leading to a negligible contribution of hard sphere interactions to the osmotic pressure of the cytoplasm. Thus, while the minimum volume of cells is primarily determined by proteins, the pressure is governed by intracellular ions.

6.3.3 Bulk modulus of cells

The *Π*-*V* relationship allows us to directly calculate the bulk (osmotic) modulus of living cells, as $B=-V\mathrm{d}\Pi/\mathrm{d}V$. We find that the bulk modulus increases with the applied osmotic pressure, and agrees very well with the hard-sphere equation of state, $B=\Pi V/(V-V_{min})$, as shown in Figure 6.3. Interestingly, this good agreement further confirms that a living cell under compression can be well described as a Van der Waals gas without interactions. We note that the bulk modulus is on the order of MPa, which is much greater than cell's shear modulus [4, 12].

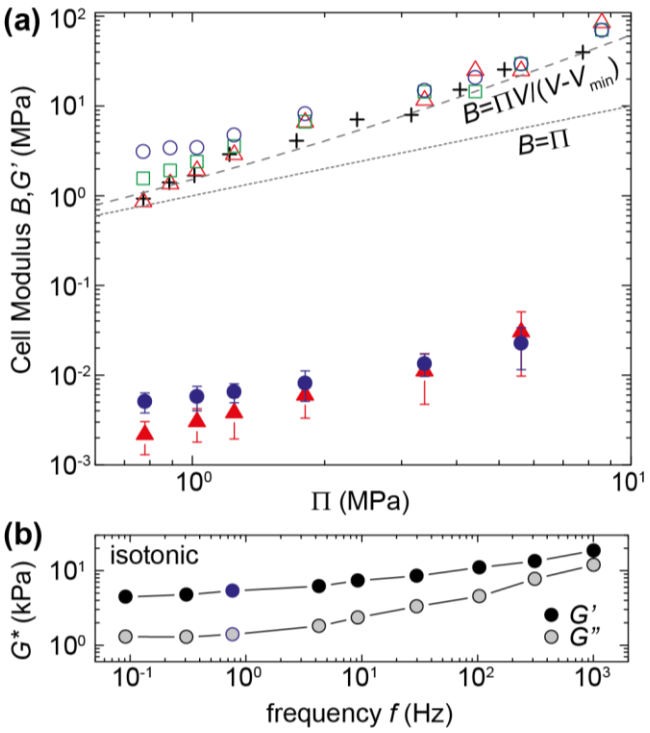

Figure 6.3 **(A)** Bulk moduli *B* calculated from the *Π-V* relationship and shear moduli *G'* measured with OMTC are plotted as a function of osmotic pressure for A7 cells, cultured on substrates with a shear modulus of 1 kPa (red triangle), 6 kPa (green square) and 20 kPa (blue circles). **(B)** *G'* and *G"* of A7 cells in isotonic medium measured as a function of frequency.

For comparison, we also directly measure the cell's shear modulus using optical magnetic twisting cytometry (OMTC). With this technique, we calculate the cortical shear modulus by measure the deformation of individual cell resulting from forces applied through a magnetic bead bound on the cell surface; it has been used extensively to quantify shear modulus of cells [refs], and our results largely agree with measurements obtained by other methods, such as AFM. The measured shear modulus, however, does increase with the applied osmotic pressure, as shown previously [refs]; this may be the result of increasing cytoskeletal protein concentration when the cell volume shrinks under osmotic compression [ref]. Our measured shear modulus, as well as prior shear moduli are on the order of kPa, approximately three orders of magnitude smaller than the bulk modulus. Indeed, by analogy to an ideal gas or Van der Waals gas system, bulk modulus of living cells comes from the repulsion of intracellular osmolytes, while the shear modulus reflects the static property of

biopolymer structures. There is no reason to expect the bulk modulus to be comparable or related to the shear modulus. Instead, this observation suggests that as we apply physiologically reasonable force on cells, such as flow shear or stretch, they would change shape by not volume. Moreover, the large discrepancy between the shear modulus of the cytoskeleton and the osmotic pressure experienced by these cells justifies our assumption of equal internal and external osmotic pressure: unlike bacteria or plan cells that have strong cell walls, animal cells lack the required rigid material structures to withstand significant osmotic pressure differences across the membrane.

6.4 Summary and Outlook

Our measurement directly quantify the Π-V relationship of living cells under different conditions, and find that suspending and partially spreading cells behave as a hard sphere gas without attractive interactions under compression; this equation of state is dominated by osmotic pressure generated by intracellular ions. We directly calculate the bulk modulus of cells from this measurement, and find it of 3 orders of magnitude greater than the shear modulus which is determined by the cytoskeleton; this also suggests that the cytoskeleton is inadequate to control cell volume which is only determined by the equation of state through osmotic pressure balance. Moreover, in direct contrast to bacteria and plant cells which use cell wall to fight against osmotic pressure variation, animal cells mainly adapt to the pressure difference by changing volume.

Bibliography

[1] Gardel, M.L., et al., *Scaling of F-actin network rheology to probe single filament elasticity and dynamics.* Physical Review Letters, 2004. **93**(18).

[2] Gardel, M.L., et al., *Elastic Behavior of Cross-Linked and Bundled Actin Networks.* Science, 2004. **304**(5675): p. 1301-1305.

[3] Cunningham, C.C., et al., *Actin-binding protein requirement for cortical stability and efficient locomotion.* Science, 1992. **255**(5042): p. 325-327.

[4] Guo, M., et al., *The Role of Vimentin Intermediate Filaments in Cortical and Cytoplasmic Mechanics.* Biophysical Journal, 2013. **105**(7): p. 1562-1568.

[5] Zhou, E.H., et al., *Universal behavior of the osmotically compressed cell and its analogy to the colloidal glass transition.* Proc Natl Acad Sci U S A, 2009. **106**(26): p. 10632-7.

[6] Pelham, R.J. and Y.L. Wang, *Cell locomotion and focal adhesions are regulated by substrate flexibility.* Proc Natl Acad Sci U S A, 1997. **94**(25): p. 13661-13665.

[7] Kasza, K.E., et al., *Filamin A Is Essential for Active Cell Stiffening but not Passive Stiffening under External Force.* Biophysical Journal, 2009. **96**(10): p. 4326-4335.

[8] Engler, A., et al., *Substrate compliance versus ligand density in cell on gel responses.* Biophysical Journal, 2004. **86**(1): p. 617-628.

[9] Valentine, M.T., et al., *Colloid surface chemistry critically affects multiple particle tracking measurements of biomaterials.* Biophysical Journal, 2004. **86**(6): p. 4004-4014.

[10] Veigel, C., et al., *The stiffness of rabbit skeletal actomyosin cross-bridges determined with an optical tweezers transducer.* Biophysical Journal, 1998. **75**(3): p. 1424-1438.

[11] Mizuno, D., et al., *Nonequilibrium mechanics of active cytoskeletal networks.* Science, 2007. **315**(5810): p. 370-373.

[12] Fabry, B., et al., *Scaling the microrheology of living cells.* Phys Rev Lett, 2001. **87**(14): p. 148102.

[13] Mijailovich, S.M., et al., *A finite element model of cell deformation during magnetic bead twisting.* Journal of Applied Physiology, 2002. **93**(4): p. 1429-1436.

[14] Fabry, B., et al., *Time course and heterogeneity of contractile responses in*

cultured human airway smooth muscle cells. J Appl Physiol, 2001. **91**(2): p. 986-94.

[15] Byfield, F.J., et al., *Absence of Filamin A Prevents Cells from Responding to Stiffness Gradients on Gels Coated with Collagen but not Fibronectin.* Biophysical Journal, 2009. **96**(12): p. 5095-5102.

[16] Chudakov, D.M., S. Lukyanov, and K.A. Lukyanov, *Tracking intracellular protein movements using photoswitchable fluorescent proteins PS-CFP2 and Dendra2.* Nature Protocols, 2007. **2**(8): p. 2024-2032.

[17] Ehrlicher, A.J., et al., *Mechanical strain in actin networks regulates FilGAP and integrin binding to filamin A.* Nature, 2011. **478**(7368): p. 260-U154.

[18] Grin, B., et al., *Withaferin a alters intermediate filament organization, cell shape and behavior.* PLoS One, 2012. **7**(6): p. e39065.

[19] Helfand, B.T., et al., *Vimentin organization modulates the formation of lamellipodia.* Mol Biol Cell, 2011. **22**(8): p. 1274-89.

[20] Mahammad, S., et al., *Giant axonal neuropathy-associated gigaxonin mutations impair intermediate filament protein degradation.* J Clin Invest, 2013. **123**(5): p. 1964-75.

[21] Bruce Alberts, A.J., Julian Lewis, Martin Raff, Keith Roberts, and Peter Walter., *Molecular Biology of the Cell*. 5th ed2007, New York: Garland Science.

[22] Carlier, M.F., *ROLE OF NUCLEOTIDE HYDROLYSIS IN THE DYNAMICS OF ACTIN-FILAMENTS AND MICROTUBULES.* International Review of Cytology-a Survey of Cell Biology, 1989. **115**: p. 139-170.

[23] Herrmann, H., et al., *Intermediate filaments: from cell architecture to nanomechanics.* Nature Reviews Molecular Cell Biology, 2007. **8**(7): p. 562-573.

[24] Janmey, P.A., et al., *Viscoelastic properties of vimentin compared with other filamentous biopolymer networks.* Journal of Cell Biology, 1991. **113**(1): p. 155-160.

[25] Sivaramakrishnan, S., et al., *Micromechanical properties of keratin intermediate filament networks.* Proceedings of the National Academy of Sciences of the United States of America, 2008. **105**(3): p. 889-894.

[26] Qin, Z., L. Kreplak, and M.J. Buehler, *Hierarchical Structure Controls Nanomechanical Properties of Vimentin Intermediate Filaments.* PLoS One, 2009. **4**(10).

[27] Bornheim, R., et al., *A dominant vimentin mutant upregulates Hsp70 and the activity of the ubiquitin-proteasome system, and causes posterior cataracts in transgenic mice.* Journal of Cell Science, 2008. **121**(22): p. 3737-3746.

[28] Gallanti, A., et al., *Desmin and vimentin as markers of regeneration in muscle*

diseases. Acta Neuropathologica, 1992. **85**(1): p. 88-92.

[29] Brenner, M., et al., *Mutations in GFAP, encoding glial fibrillary acidic protein, are associated with Alexander disease.* Nature Genetics, 2001. **27**(1): p. 117-120.

[30] Chamcheu, J.C., et al., *Keratin gene mutations in disorders of human skin and its appendages.* Arch Biochem Biophys, 2011. **508**(2): p. 123-37.

[31] Perrot, R., et al., *Review of the multiple aspects of neurofilament functions, and their possible contribution to neurodegeneration.* Mol Neurobiol, 2008. **38**(1): p. 27-65.

[32] Perrot, R. and J. Eyer, *Neuronal intermediate filaments and neurodegenerative disorders.* Brain Res Bull, 2009. **80**(4-5): p. 282-95.

[33] Omary, M.B., P.A. Coulombe, and W.H.I. McLean, *Mechanisms of disease: Intermediate filament proteins and their associated diseases.* New England Journal of Medicine, 2004. **351**(20): p. 2087-2100.

[34] Hofmann, I., H. Herrmann, and W.W. Franke, *Assembly and structure of calcium-induced thick vimentin filaments.* Eur J Cell Biol, 1991. **56**(2): p. 328-41.

[35] Lin, Y.C., et al., *Divalent Cations Crosslink Vimentin Intermediate Filament Tail Domains to Regulate Network Mechanics.* Journal of Molecular Biology, 2010. **399**(4): p. 637-644.

[36] Desprat, N., et al., *Creep function of a single living cell.* Biophysical Journal, 2005. **88**(3): p. 2224-2233.

[37] Alcaraz, J., et al., *Microrheology of human lung epithelial cells measured by atomic force microscopy.* Biophysical Journal, 2003. **84**(3): p. 2071-2079.

[38] Lau, A.W.C., et al., *Microrheology, stress fluctuations, and active behavior of living cells.* Physical Review Letters, 2003. **91**(19).

[39] Nekrasova, O.E., et al., *Vimentin intermediate filaments modulate the motility of mitochondria.* Mol Biol Cell, 2011. **22**(13): p. 2282-9.

[40] Chang, L., et al., *The dynamic properties of intermediate filaments during organelle transport.* J Cell Sci, 2009. **122**(Pt 16): p. 2914-23.

[41] Gao, Y. and E. Sztul, *A novel interaction of the Golgi complex with the vimentin intermediate filament cytoskeleton.* J Cell Biol, 2001. **152**(5): p. 877-94.

[42] Gao, Y.S., et al., *A novel type of regulation of the vimentin intermediate filament cytoskeleton by a Golgi protein.* Eur J Cell Biol, 2002. **81**(7): p. 391-401.

[43] Styers, M.L., A.P. Kowalczyk, and V. Faundez, *Intermediate filaments and vesicular membrane traffic: the odd couple's first dance?* Traffic, 2005. **6**(5): p. 359-65.

[44] Styers, M.L., et al., *The endo-lysosomal sorting machinery interacts with the intermediate filament cytoskeleton.* Mol Biol Cell, 2004. **15**(12): p. 5369-82.

[45] Wang, N., J.D. Tytell, and D.E. Ingber, *Mechanotransduction at a distance: mechanically coupling the extracellular matrix with the nucleus.* Nature Reviews Molecular Cell Biology, 2009. **10**(1): p. 75-82.

[46] Fletcher, D.A. and D. Mullins, *Cell mechanics and the cytoskeleton.* Nature, 2010. **463**(7280): p. 485-492.

[47] Ingber, D.E., *Mechanobiology and diseases of mechanotransduction.* Annals of Medicine, 2003. **35**(8): p. 564-577.

[48] Mendez, M.G., S.I. Kojima, and R.D. Goldman, *Vimentin induces changes in cell shape, motility, and adhesion during the epithelial to mesenchymal transition.* Faseb Journal, 2010. **24**(6): p. 1838-1851.

[49] Eckes, B., et al., *Impaired mechanical stability, migration and contractile capacity in vimentin-deficient fibroblasts.* Journal of Cell Science, 1998. **111**: p. 1897-1907.

[50] Rogel, M.R., et al., *Vimentin is sufficient and required for wound repair and remodeling in alveolar epithelial cells.* Faseb Journal, 2011. **25**(11): p. 3873-3883.

[51] Koster, S., et al., *Nanomechanics of vimentin intermediate filament networks.* Soft Matter, 2010. **6**(9): p. 1910-1914.

[52] Howard, J., *Mechanics of motor proteins and the cytoskeleton*2001, Sunderland, MA 01375 USA: Sinauer Associates, Inc.

[53] Vale, R.D., *The molecular motor toolbox for intracellular transport.* Cell, 2003. **112**(4): p. 467-480.

[54] Svoboda, K. and S.M. Block, *Force and velocity measured for single kinesin molecules.* Cell, 1994. **77**(5): p. 773-784.

[55] Rai, A.K., et al., *Molecular Adaptations Allow Dynein to Generate Large Collective Forces inside Cells.* Cell, 2013. **152**(1-2): p. 172-182.

[56] Hendricks, A.G., E.L.F. Holzbaur, and Y.E. Goldman, *Force measurements on cargoes in living cells reveal collective dynamics of microtubule motors.* Proceedings of the National Academy of Sciences of the United States of America, 2012. **109**(45): p. 18447-18452.

[57] Doyle, A.D. and K.M. Yamada, *CELL BIOLOGY Sensing tension.* Nature, 2010. **466**(7303): p. 192-193.

[58] Grashoff, C., et al., *Measuring mechanical tension across vinculin reveals regulation of focal adhesion dynamics.* Nature, 2010. **466**(7303): p. 263-U143.

[59] Dufrene, Y.F., et al., *Five challenges to bringing single-molecule force spectroscopy into living cells.* Nature Methods, 2011. **8**(2): p. 123-127.

[60] Gundersen, Gregg G. and Howard J. Worman, *Nuclear Positioning.* Cell, 2013. **152**(6): p. 1376-1389.

[61] Heisenberg, C.-P. and Y. Bellaïche, *Forces in Tissue Morphogenesis and Patterning.* Cell, 2013. **153**(5): p. 948-962.

[62] Han, W.P., et al., *Neuropeptide release by efficient recruitment of diffusing cytoplasmic secretory vesicles.* Proceedings of the National Academy of Sciences of the United States of America, 1999. **96**(25): p. 14577-14582.

[63] Kyoung, M. and E.D. Sheets, *Vesicle Diffusion Close to a Membrane: Intermembrane Interactions Measured with Fluorescence Correlation Spectroscopy.* Biophysical Journal, 2008. **95**(12): p. 5789-5797.

[64] del Alamo, J.C., et al., *Anisotropic rheology and directional mechanotransduction in vascular endothelial cells.* Proc Natl Acad Sci U S A, 2008. **105**(40): p. 15411-15416.

[65] Jaqaman, K., et al., *Cytoskeletal Control of CD36 Diffusion Promotes Its Receptor and Signaling Function.* Cell, 2011. **146**(4): p. 593-606.

[66] Hammar, P., et al., *The lac Repressor Displays Facilitated Diffusion in Living Cells.* Science, 2012. **336**(6088): p. 1595-1598.

[67] Ananthanarayanan, V., et al., *Dynein Motion Switches from Diffusive to Directed upon Cortical Anchoring.* Cell, 2013. **153**(7): p. 1526-1536.

[68] Brangwynne, C.P., et al., *Cytoplasmic diffusion: molecular motors mix it up.* Journal of Cell Biology, 2008. **183**(4): p. 583-587.

[69] Wu, P.H., et al., *High-throughput ballistic injection nanorheology to measure cell mechanics.* Nature Protocols, 2012. **7**(1): p. 155-170.

[70] Yamada, S., D. Wirtz, and S.C. Kuo, *Mechanics of living cells measured by laser tracking microrheology.* Biophysical Journal, 2000. **78**(4): p. 1736-1747.

[71] Baker, E.L., et al., *Cancer Cell Stiffness: Integrated Roles of Three-Dimensional Matrix Stiffness and Transforming Potential.* Biophysical Journal, 2010. **99**(7): p. 2048-2057.

[72] Gupton, S.L., et al., *Cell migration without a lamellipodium: translation of actin dynamics into cell movement mediated by tropornyosin.* Journal of Cell Biology, 2005. **168**(4): p. 619-631.

[73] Hale, C.M., S.X. Sun, and D. Wirtz, *Resolving the Role of Actoymyosin Contractility in Cell Microrheology.* PLoS One, 2009. **4**(9).

[74] MacKintosh, F.C., *Active diffusion: The erratic dance of chromosomal loci.* Proceedings of the National Academy of Sciences of the United States of America, 2012. **109**(19): p. 7138-7139.

[75] Hoffman, B.D., et al., *The consensus mechanics of cultured mammalian cells.* Proceedings of the National Academy of Sciences, 2006. **103**(27): p. 10259-10264.

[76] Weber, S.C., A.J. Spakowitz, and J.A. Theriot, *Nonthermal ATP-dependent fluctuations contribute to the in vivo motion of chromosomal loci.* Proc Natl Acad Sci U S A, 2012. **109**(19): p. 7338-7343.

[77] Parry, B.R., et al., *The Bacterial Cytoplasm Has Glass-like Properties and Is Fluidized by Metabolic Activity.* Cell, 2014. **156**(1-2): p. 183-194.

[78] MacKintosh, F.C. and A.J. Levine, *Nonequilibrium mechanics and dynamics of motor-activated gels.* Physical Review Letters, 2008. **100**(1).

[79] Koenderink, G.H., et al., *An active biopolymer network controlled by molecular motors.* Proceedings of the National Academy of Sciences of the United States of America, 2009. **106**(36): p. 15192-15197.

[80] Brangwynne, C.P., et al., *Nonequilibrium microtubule fluctuations in a model cytoskeleton.* Physical Review Letters, 2008. **100**(11).

[81] Mizuno, D., et al., *High-Resolution Probing of Cellular Force Transmission.* Physical Review Letters, 2009. **102**(16): p. 168102.

[82] Kovacs, M., et al., *Mechanism of blebbistatin inhibition of myosin II.* Journal of Biological Chemistry, 2004. **279**(34): p. 35557-35563.

[83] Cross, S.E., et al., *Nanomechanical analysis of cells from cancer patients.* Nature Nanotechnology, 2007. **2**(12): p. 780-783.

[84] Plodinec, M., et al., *The Nanomechanical Signature of Breast Cancer.* Biophysical Journal, 2013. **104**(2): p. 321A-321A.

[85] Kraning-Rush, C.M., J.P. Califano, and C.A. Reinhart-King, *Cellular Traction Stresses Increase with Increasing Metastatic Potential.* PLoS One, 2012. **7**(2).

[86] Nagaraja, G.M., et al., *Gene expression signatures and biomarkers of noninvasive and invasive breast cancer cells: comprehensive profiles by representational difference analysis, microarrays and proteomics.* Oncogene, 2006. **25**(16): p. 2328-2338.

[87] Chan, S.W., et al., *A role for TAZ in migration, invasion, and tumorigenesis of breast cancer cells.* Cancer Research, 2008. **68**(8): p. 2592-2598.

[88] Holzer, R., et al., *Development and Characterization of a Progressive Series of Mammary Adenocarcinoma Cell Lines Derived from the C3(1)/SV40 Large T-antigen Transgenic Mouse Model.* Breast Cancer Research and Treatment, 2003. **77**(1): p. 65-76.

[89] DeBerardinis, R.J., et al., *Brick by brick: metabolism and tumor cell growth.* Current Opinion in Genetics & Development, 2008. **18**(1): p. 54-61.

[90] Sherr, C.J., *Cancer cell cycles.* Science, 1996. **274**(5293): p. 1672-1677.

[91] Discher, D.E., P. Janmey, and Y.L. Wang, *Tissue cells feel and respond to the stiffness of their substrate.* Science, 2005. **310**(5751): p. 1139-43.

[92] Solon, J., et al., *Fibroblast adaptation and stiffness matching to soft elastic*

substrates. Biophysical Journal, 2007. **93**(12): p. 4453-4461.

[93] Engler, A.J., et al., *Matrix elasticity directs stem cell lineage specification.* Cell, 2006. **126**(4): p. 677-89.

[94] Fu, J., et al., *Mechanical regulation of cell function with geometrically modulated elastomeric substrates.* Nature Methods, 2010. **7**(9): p. 733-U95.

[95] Huebsch, N., et al., *Harnessing traction-mediated manipulation of the cell/matrix interface to control stem-cell fate.* Nature Materials, 2010. **9**(6): p. 518-526.

[96] Saha, K., et al., *Substrate Modulus Directs Neural Stem Cell Behavior.* Biophysical Journal, 2008. **95**(9): p. 4426-4438.

[97] Dupont, S., et al., *Role of YAP/TAZ in mechanotransduction.* Nature, 2011. **474**(7350): p. 179-U212.

[98] Evans, N.D., et al., *Substrate stiffness affects early differentiation events in embryonic stem cells.* European Cells & Materials, 2009. **18**: p. 1-14.

[99] Tee, S.Y., et al., *Cell Shape and Substrate Rigidity Both Regulate Cell Stiffness.* Biophysical Journal, 2011. **100**(5): p. L25-L27.

[100] McBeath, R., et al., *Cell shape, cytoskeletal tension, and RhoA regulate stem cell lineage commitment.* Developmental Cell, 2004. **6**(4): p. 483-495.

[101] Tzur, A., et al., *Cell Growth and Size Homeostasis in Proliferating Animal Cells.* Science, 2009. **325**(5937): p. 167-171.

[102] Stewart, M.P., et al., *Hydrostatic pressure and the actomyosin cortex drive mitotic cell rounding.* Nature, 2011. **469**(7329): p. 226-230.

[103] Wang, N., et al., *Micropatterning tractional forces in living cells.* Cell Motil Cytoskeleton, 2002. **52**(2): p. 97-106.

[104] Larson, R.G., *The structure and rheology of complex fluids*1999: Oxford University Press.

[105] Tharmann, R., M.M.A.E. Claessens, and A.R. Bausch, *Viscoelasticity of Isotropically Cross-Linked Actin Networks.* Physical Review Letters, 2007. **98**(8): p. 088103.

[106] MacKintosh, F.C., J. Käs, and P.A. Janmey, *Elasticity of Semiflexible Biopolymer Networks.* Physical Review Letters, 1995. **75**(24): p. 4425-4428.

[107] Lang, F., et al., *Functional significance of cell volume regulatory mechanisms.* Physiological Reviews, 1998. **78**(1): p. 247-306.

[108] Sheng, H.P. and R.A. Huggins, *Review of body-composition studies with emphasis on total-body water and fat.* American Journal of Clinical Nutrition, 1979. **32**(3): p. 630-647.

[109] Dhar, A., et al., *Structure, function, and folding of phosphoglycerate kinase are strongly perturbed by macromolecular crowding.* Proc Natl Acad Sci U S A,

2010. **107**(41): p. 17586-17591.

[110] Ball, P., *Water as an active constituent in cell biology.* Chemical Reviews, 2008. **108**(1): p. 74-108.

[111] Minton, A.P., *The influence of macromolecular crowding and macromolecular confinement on biochemical reactions in physiological media.* Journal of Biological Chemistry, 2001. **276**(14): p. 10577-10580.

[112] Hazel, J., et al., *Changes in Cytoplasmic Volume Are Sufficient to Drive Spindle Scaling.* Science, 2013. **342**(6160): p. 853-856.

[113] Good, M.C., et al., *Cytoplasmic Volume Modulates Spindle Size During Embryogenesis.* Science, 2013. **342**(6160): p. 856-860.

[114] Ellis, R.J., *Macromolecular crowding: obvious but underappreciated.* Trends in Biochemical Sciences, 2001. **26**(10): p. 597-604.

[115] Robbins, E., T. Pederson, and P. Klein, *Comparison of mitotic phenomena and effects induced by hypertonic solutions in HeLa cells.* Journal of Cell Biology, 1970. **44**(2): p. 400-416.

[116] Chowdhury, F., et al., *Material properties of the cell dictate stress-induced spreading and differentiation in embryonic stem cells.* Nature Materials, 2010. **9**(1): p. 82-88.

[117] Trappmann, B., et al., *Extracellular-matrix tethering regulates stem-cell fate.* Nature Materials, 2012. **11**(7): p. 642-649.